Materials Advances

ROYAL SOCIETY OF CHEMISTRY

PAPER

View Article Online
View Journal | View Issue

Cite this: *Mater. Adv.*, 2025, **6**, 4438

Development, characterisation and neuroprotective effects of polymer–drug conjugate nano-polyplex: working towards a multi-target treatment for neurodegenerative diseases†

Nuruddin Mahadik, Gemma A. Barron, Paul Kong Thoo Lin and Colin J. Thompson *

Neurodegenerative diseases (NDs) are complex, multifaceted conditions that require novel, multi-targeted therapeutic approaches. This study aimed to develop a multifunctional polymer–drug conjugate (PDC) by employing a novel strategy of utilizing PDC-based nano-polyplexes as a multi-target treatment for NDs. The nano-polyplex (N5NM15) was formulated by combining polyallylamine hydrochloride-vanillin (NM15) and polyacrylic acid–naphthalimidohexylamine (N5) conjugates. Antioxidant capacity was measured *via* ORAC assay, and cholinesterase inhibition was evaluated using Ellman's assay. Cytotoxicity, neuroprotective effects, and anti-inflammatory activity were tested in undifferentiated SH-SY5Y and BV-2 cells *via* MTT assay. Amyloid-beta aggregation was assessed using Thioflavin T assay and TEM imaging in a cell-free system. The results demonstrated that N5NM15 resulted in uniform nanoparticles with an average size of 30.5 ± 7.9 nm, confirmed *via* cryo-TEM. Cytotoxicity studies indicated high biocompatibility with SH-SY5Y cells (viability >90%) and moderate toxicity in BV-2 cells (viability 75%, $p \leq 0.001$). Furthermore, N5NM15 demonstrated significantly enhanced *in vitro* antioxidant activity ($p \leq 0.001$, after adjustment) and cholinesterase inhibition ($p \leq 0.0001$ for AChE and $p \leq 0.01$ for BuChE, after adjustment) compared to starting materials. N5NM15 also protected SH-SY5Y cells from hydrogen peroxide-induced oxidative stress ($p \leq 0.0001$), reduced lipopolysaccharide-induced inflammation in BV-2 cells ($p \leq 0.05$), inhibited BuChE activity in SH-SY5Y cells ($p \leq 0.01$), and reduced amyloid-beta aggregation ($p \leq 0.01$). Notably, polyacrylic acid demonstrated protective and anti-inflammatory effects in both cell lines ($p \leq 0.0001$) and inhibited amyloid-beta aggregation ($P \leq 0.001$). These findings suggest the potential use of N5NM15 and polyacrylic acid as treatment options for NDs.

Received 24th February 2025,
Accepted 29th May 2025

DOI: 10.1039/d5ma00174a

rsc.li/materials-advances

1. Introduction

Neurodegenerative diseases (NDs) pose a growing global healthcare challenge, marked by the progressive loss of neurons resulting in impairments such as dementia and motor dysfunction.[1,2] NDs like Alzheimer's disease (AD), amyotrophic lateral sclerosis (ALS), Parkinson's disease (PD), and Huntington's disease (HD) significantly impact both individuals and society.[1,2]

These NDs have diverse pathophysiological features, some affecting memory, and cognition, whilst others can affect a person's ability to move, speak, and/or breathe.[2] The pathogenesis of NDs are complex, involving genetic, environmental, and lifestyle factors.[2,3] Common mechanisms include protein misfolding and aggregation, mitochondrial dysfunction, impaired protein clearance, neuroinflammation, and oxidative stress (OS).[4] Despite these common mechanisms, the molecular pathways differ across NDs, complicating treatment efforts. Current therapies focus on single targets and typically manage symptoms rather than stop the progression of the disease. For example, cholinesterase inhibitors and NMDA receptor antagonists are used in AD,[3] whilst dopaminergic drugs and monoamine oxidase-B inhibitors are typically used in PD.[5] Recent

School of Pharmacy, Applied Sciences and Public Health, Robert Gordon University, Aberdeen, UK AB10 7GJ. E-mail: c.thompson@rgu.ac.uk

† Electronic supplementary information (ESI) available: A translucent and clear solution of N5NM15, MTT cell viability assay of Tris–HCl buffer (pH 7.4), HEXNAP in undifferentiated SH-SY5Y and BV-2 cells, Ellman's BuChE kinetic study of N5NM15 nano-polyplex at a concentration of 44 μg mL^{-1}; MTT cell viability assay of H_2O_2 in undifferentiated SH-SY5Y cells and BV-2 cells; MTT cell viability assay of LPS in BV-2 cells (DOC). See DOI: https://doi.org/10.1039/d5ma00174a

developments, such as monoclonal antibodies targeting amyloid plaques in AD, have shown promise but have limited efficacy thus, highlighting the need for continued research and development.[3,6,7]

In recent years,[8,9] there has been a growing consensus that multi-target treatments may provide substantial benefits in treating NDs such as AD.[10] By combining two or more pharmacophores into a single compound, this approach can potentially be more comprehensive and effective in managing the disease.[10] However, these multi-target compounds often face challenges, including low water-solubility and toxicity, which result in low bioavailability.[11,12]

One of the strategies to address these challenges is to develop polymer–drug conjugates (PDCs). These are therapeutic compounds where drugs are covalently attached to water-soluble polymers, thereby enhancing pharmacokinetic properties, such as stability, solubility, half-life, and bioavailability.[3] Our previous study[13] focused on the synthesis and characterisation of novel water-soluble polyallylamine hydrochloride-vanillin (NM15) and polyacrylic acid–naphthalimidohexylamine (N5) conjugates (Fig. 1(A) and (B)). NM15 was synthesised by Schiff base condensation between the primary amine groups of polyallylamine hydrochloride and the aldehyde group of vanillin, while N5 was obtained *via* EDC/NHS-mediated coupling of polyacrylic acid with naphthalimidohexylamine (HEXNAP) (Fig. S1 and S2, ESI† for schematic representation of the chemical synthesis). The findings demonstrated that NM15 significantly enhanced *in vitro* antioxidant activity ($p \leq 0.0001$) compared to vanillin, while N5 significantly exhibited cholinesterase inhibitory activity against acetylcholinesterase (AChE) and butyrylcholinesterase (BuChE) ($p \leq 0.0001$) compared to HEXNAP. Furthermore, kinetic and molecular modelling studies revealed N5 to be a competitive inhibitor of BuChE which interacts with the active sites of human AChE and BuChE enzymes. Based on these findings, NM15 and N5 were identified as lead PDCs, highlighting their potential as multi-target therapeutic candidates for NDs.[13]

A novel approach for designing PDC combinations involves developing polyelectrolyte complexes (PECs) between two distinct polymers with opposing charges, each conjugated to a different drug. PECs are formed through strong electrostatic (Coulomb's) interactions between oppositely charged polyelectrolytes.[14] These opposing charges enable the formation of nano-polyplexes, allowing for the simultaneous delivery of both active moieties in a single formulation (Fig. 1(C)). This PDC-based nano-polyplex approach has the potential to address the multifactorial aetiology of NDs by employing a multi-target approach. However, this strategy of developing PDC-based nano-polyplex has yet to be explored as a multi-target treatment for NDs and other diseases.

Therefore, this research has focused on the formulation, characterisation, and *in vitro* evaluation of novel PDC nano-polyplexes for the treatment of NDs. The objectives were to: (i) formulate and characterise novel nano-polyplexes combining NM15 and N5 conjugates, (ii) assess novel conjugates/nano-polyplexes cytotoxicity in undifferentiated human SH-SY5Y neuroblastoma and murine BV-2 microglial cell lines using the MTT assay, (iii) evaluate *in vitro* antioxidant and cholinesterase inhibitory activity of novel conjugates/nano-polyplexes using oxygen radical absorbance capacity (ORAC) assay and Ellman's assay, (iv) assess the neuroprotective and anti-inflammatory properties of the novel conjugates/nano-polyplexes against hydrogen peroxide (H_2O_2) and lipopolysaccharide (LPS) stressors in undifferentiated SH-SY5Y and BV-2 cells using the MTT assay, (v) evaluate *in vitro* cholinesterase inhibitory activity of novel conjugates/nano-polyplexes in undifferentiated SH-SY5Y using Ellman's assay, and (vi) determine the inhibitory effects of the novel nano-polyplex on amyloid-beta (Aβ) aggregation activity using Thioflavin T (ThT) assay. This multifaceted approach sought to introduce novel therapeutic strategies for NDs. The outcomes could significantly contribute to advancing therapies in neurological disorders.

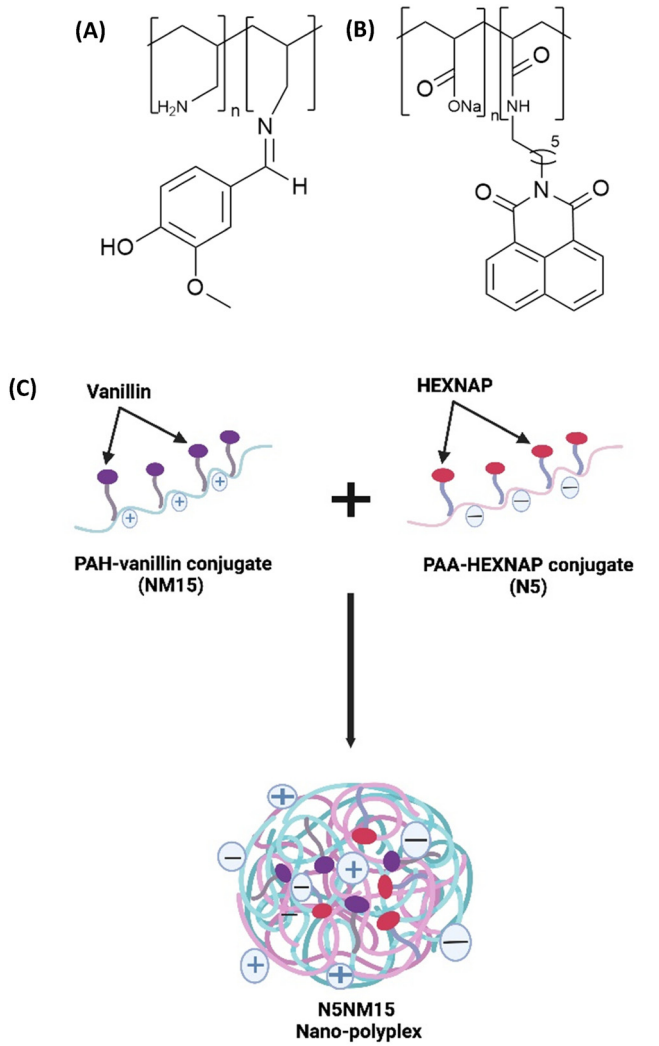

Fig. 1 Chemical structures of (A) NM15 and (B) N5. (C) Schematic representation of the formation of a nano-polyplex (N5NM15) between N5 and NM15 in solution.

2. Materials and methods

2.1 Materials

Polyallylamine hydrochloride (M_W = 17 500 g mol^{-1}), vanillin, Trolox, *N*-acetyl cysteine, *Electrophorus electricus*, equine serum (5,5′-dithiobis-(2-nitrobenzoic acid)) (DTNB), sodium phosphate, HEPES, acetylthiocholine iodide, and butyrylthiocholine iodide, 3-(4,5-dimethyl-2-thiazolyl)-2,5-diphenyl-2*H*-tetrazolium Bromide (MTT), 2,2′-azobis(2-methylpropionamidine) dihydrochloride (AAPH), lipopolysaccharide (*Escherichia coli* O111:B4, L2630), hydrogen peroxide, thioflavin T (ThT), and β-amyloid peptide (1–42, PP69) were purchased from Sigma Aldrich (Dorset, UK). Polyacrylic acid (M_W = 25 000 g mol^{-1}) was purchased from Fujifilm Wako Pure Chemical Corporation (Osaka, Japan). Tris(hydroxymethyl)aminomethane hydrochloride (Tris–HCl), dimethyl sulfoxide (DMSO), fluorescein sodium salt, and Oxoid phosphate buffered saline tablets (Dulbecco A) were purchased from Fisher Scientific (UK). DMEM media (Cat-no 41966052), trypsin-EDTA (0.05%) (Cat-no 25300054), penicillin–streptomycin (Pen/Strep, 10 000 U mL^{-1}) (Cat no 15140122), fetal bovine serum (FBS, Cat-no A5256801), MEM non-essential amino acids solution (NEAA, Cat-no 11140050) were purchased from ThermoFisher Scientific (UK). The undifferentiated SH-SY5Y human neuroblastoma cell line was purchased from the European Collection of Authenticated Cell Cultures (ECACC), and the BV-2 murine microglial cell line was purchased from Stratech Scientific Ltd (UK).

2.2 Methods

2.2.1 Development of nano-polyplex. Nano-polyplexes of NM15 and N5 were formulated by gradually mixing a fixed concentration of NM15 with varying mass ratios of N5 (2 : 1, 3.5 : 1, 7.5 : 1, and 10 : 1) in 10 mM Tris–HCl buffer (pH 7.4), resulting in the formation of N5NM15 nano-polyplex. Similarly, PAANM15 nano-polyplex was formulated by gradually mixing a fixed concentration of NM15 with varying mass ratios of PAA (1 : 1, 5 : 1, 7.5 : 1, and 10 : 1) in 10 mM Tris–HCl buffer (pH 7.4), resulting in the formation of PAANM15 nano-polyplex.

2.2.2 Characterization of nano-polyplex

2.2.2.1 Dynamic light scattering. The particle size (hydrodynamic diameter) and polydispersity index (PDI) of the nano-polyplexes were determined using a dynamic light scattering (DLS) particle size analyzer (Zetasizer Nano-ZS, Malvern Instruments, Worcestershire, UK). A 1 mL aliquot of each sample solution was transferred into a DTS0012 disposable sizing cuvette and placed in a thermostatic chamber at 25 °C. The light scattering measurements were carried out using a 50-mV laser at a 90° angle. The data obtained were processed using the Zetasizer software. In addition, the zeta potential of the selected lead nano-polyplex ratio was measured using DTS1070 disposable folded capillary cells on the same instrument.

2.2.2.2 Cryogenic-transmission electron microscopy. Prior to imaging, grids were prepared in a glow discharger. The lead nano-polyplex samples were blotted and frozen onto Lacey carbon grids (EMResolutions, UK) using a Leica GP2 plunge freezer. The samples were then imaged using a JEOL 2100Plus transmission electron microscope (TEM) (JEOL, Japan) equipped with a Gatan UltraScan camera. Imaging was performed at a magnification of 15 000× to capture the detailed shape and size of the nano-polyplexes. Particle size measurements were performed using ImageJ software.

2.2.3 Cellular toxicity: MTT assay

2.2.3.1 General cell culture technique. Cells were cultured according to the methods of Smith *et al.*[15] and Tao *et al.*,[16] with minor modifications. Undifferentiated human SH-SY5Y and murine BV-2 microglial cell lines were maintained in Dulbecco's modified Eagle's medium (DMEM) supplemented with 10% (v/v) FBS, 1% (v/v) NEAA, and 1% (v/v) penicillin/streptomycin. Cells were grown in T25 flasks in a humidified incubator at 37 °C with 5% CO_2. Upon reaching 80% confluence, cells were passaged, centrifuged, counted, and seeded into appropriate 96-well plates (Cat-no 167008) or flasks for further experiments.

2.2.3.2 MTT assay. The MTT assay was carried out as previously reported by Barron *et al.*,[17] with minor modifications. Cells were seeded into 96-well plates (10 000 undifferentiated SH-SY5Y cells in 100 μL per well and 5000 BV2 cells in 100 μL per well) and incubated for 24 h at 37 °C with 5% CO_2 to allow for attachment. A dilution series of NM15 (4–1000 μg mL^{-1}, tested only on SH-SY5Y cells), N5 (2–250 μg mL^{-1}), and N5NM15 with a fixed concentration of NM15 (12.5 μg mL^{-1}) and varying mass ratios of N5 (2 : 1 (25 : 12.5 μg mL^{-1}), 3.5 : 1 (44 : 12.5 μg mL^{-1}), 5 : 1 (62.5 : 12.5 μg mL^{-1}), 7.5 : 1 (94 : 12.5 μg mL^{-1})) was prepared in serum-free DMEM. These solutions were made from stock solutions prepared in 10 mM Tris–HCl buffer (pH 7.4) (solvent control). A dilution series of naphthalimidohexylamine (HEXNAP, 0.1–25 μg mL^{-1}) was also prepared in serum-free DMEM from 100 μg mL^{-1} stock solutions in 10 mM Tris–HCl buffer (pH 7.4). The HEXNAP stock solution in buffer was prepared from a 50 mg mL^{-1} stock solution in DMSO, due to HEXNAP being soluble only in organic solvents. All compounds were added to the corresponding wells (100 μL per well in 6 technical replicates) after the serum-containing DMEM was removed from the wells for the undifferentiated SH-SY5Y cells only. After 24 h incubation at 37 °C with 5% CO_2, the serum-free DMEM was removed per well, and 100 μL sterile-filtered (0.22 μm) MTT solution (1 mg mL^{-1} in serum-free DMEM) was added to each well, ensuring the procedure was performed in the dark. The plates were then incubated for 4 h at 37 °C with 5% CO_2. After this incubation, MTT solution was removed, and 200 μL DMSO was added to each well. The plates were shaken in the dark at room temperature for 15 min, and absorbance was measured at 595 nm (BioTek Synergy HT microplate reader, Agilent, UK). The percentage absorbance, representing cell viability, was calculated relative to the solvent control (100% cell viability).

2.2.4 Antioxidant activity: oxygen radical absorbance capacity assay. The oxygen radical absorbance capacity (ORAC) assay was carried out as previously reported by Huang *et al.*,[18] with minor modifications. Using a black-walled 96-well plate, a fixed

concentration of each compound (25 μL added/well in triplicate) was prepared based on the MTT results: 12.5 μg mL^{-1} for NM15, a 7.5 : 1 (94 : 12.5 μg mL^{-1}) ratio for PAANM15, and a 3.5 : 1 (44 : 12.5 μg mL^{-1}) ratio for N5NM15, all prepared in 10 mM Tris–HCl buffer (pH 7.4). Blank and no AAPH controls as well as a dilution series of vanillin (0.6–2 μg mL^{-1}) and Trolox (0.6–31 μg mL^{-1}) were also prepared (25 μL added per well in triplicate). Sodium fluorescein solution (150 μL, 25 nM,10 mM Tris–HCl buffer (pH 7.4)) was added to each well, and the plate was incubated in the dark at 37 °C for 30 min. Following incubation, 25 μL AAPH solution (0.15 M, 10 mM Tris–HCl buffer (pH 7.4)) was added to each well and for control without AAPH, 25 μL 10 mM Tris–HCl buffer (pH 7.4) was added instead. Fluorescence was measured every 2 min for 2 h (BioTek Synergy HT microplate reader, excitation at 485 nm, and emission at 525 nm). The results were expressed as milligrams of Trolox equivalent (TE) per gram of dry sample (C).

2.2.5 *In vitro* cholinesterase inhibitory activity

2.2.5.1 Ellman's assay. The inhibitory activity of N5NM15 and N5PAH against AChE and BuChE was determined using an Ellman's assay as previously reported by Blaikie *et al.*,[9] with minor modifications. AChE and BuChE stock solutions (22 U mL^{-1}) from *Electrophorus electricus* and equine serum respectively were prepared and diluted before use. A 3 mM 5,5′-dithiobis-(2-nitrobenzoic acid) (DTNB) solution was prepared in phosphate/HEPES buffer (0.05 M/0.09 M, pH 7.5). Solutions of 15 mM acetylthiocholine iodide (AChEI) and butyrylthiocholine iodide (BuChEI) were prepared in dH_2O. N5NM15 and N5PAH were prepared in 10 mM Tris–HCl buffer, pH 7.4. A dilution series of all tested compounds (8–2000 μg mL^{-1} for AChE and 0.008–2000 μg mL^{-1} for BuChE) were prepared. For the reaction to occur, 125 μL DTNB solution, 25 μL samples, negative control (Tris–HCl buffer, pH 7.4), and 25 μL diluted AChE or BuChE solution were added to a 96-well plate in triplicate. The plate was incubated for 10 min at 37 °C, then 25 μL AChEI or BuChEI solution were added to all wells, and the plate was incubated for a further 20 min. The absorbance was measured at 415 nm (BioTek Synergy HT microplate reader). The cholinesterase inhibitory activity was expressed in terms of IC_{50} (concentration at which 50% of the cholinesterase activity was inhibited compared to HEXNAP).

2.2.5.2 Kinetic study of BuChE inhibition. For the kinetic study, N5NM15 and N5PAH were examined at $IC_{50}/2$, IC_{50}, and 2^*IC_{50} (these concentrations were selected from Ellman's assay results). BuChEI substrate (5 to 50 mM) was prepared and N5NM15 and N5PAH were evaluated against each substrate concentration. The method was as described in Section 2.2.5.1 up to substrate addition when the absorbance was measured every min for 20 min at 415 nm (BioTek Synergy HT microplate reader). For each substrate concentration, absorbance was plotted against time, and the slope was taken as the rate (v). The reciprocal of substrate concentration ($1/S$) and rate ($1/v$) were plotted for each compound concentration and the negative control (10 mM Tris–HCl buffer, pH 7.4). This generated the Lineweaver–Burke plot, which could be used to determine the V_{max} and K_m values for each compound concentration and negative control.

2.2.6 Cell viability in the presence of H_2O_2 stressor using the MTT assay. The protective effects of the compounds against H_2O_2 were determined using an MTT assay as previously reported by Scipioni *et al.*,[19] with minor modifications. Briefly, undifferentiated SH-SY5Y cells (10 000 cells/100 μL per well) and BV-2 cells (2000 cells/100 μL per well) were seeded and allowed to attach for 24 h at 37 °C with 5% CO_2. Based on cell viability results, vanillin, PAH, and NAC at 12.5 μg mL^{-1}; HEXNAP at 3 μg mL^{-1}; N5 and PAA at 44 μg mL^{-1}; PAANM15 at a ratio of 7.5 : 1 (94 : 12.5 μg mL^{-1}); and N5NM15, N5PAH, and PAAPAH at a ratio of 3.5 : 1 (44 : 12.5 μg mL^{-1}) were prepared Tris–HCl buffer (10 mM, pH 7.4). Tris–HCl buffer (10 mM, pH 7.4) in serum-free media was added as the solvent control. After 24 h, H_2O_2 (275 μM; 100 μL per well) for undifferentiated SH-SY5Y cells and H_2O_2 (200 μM; 100 μL per well) for BV-2 cells were prepared in serum-free DMEM and added to all wells. For the solvent control without H_2O_2, deionized water in serum-free DMEM was added instead of H_2O_2. Following another 24 h incubation at 37 °C with 5% CO_2, the serum-free DMEM was removed, and the MTT assay was performed as described previously (Section 2.2.3) to assess cell viability. The percentage absorbance, representing cell viability, was calculated relative to the H_2O_2 control alone (100% cell viability).

2.2.7 Cell viability in the presence of LPS stressor using the MTT assay. Briefly, BV-2 cells (500 cells/100 μL per well) were seeded and allowed to attach for 24 h at 37 °C with 5% CO_2. After 24 h, 16 μg mL^{-1} LPS, was added to all the wells except to solvent control wells without LPS, where serum-free DMEM was added. The plate was then incubated for an additional 24 h at 37 °C with 5% CO_2. Subsequently, treatments were prepared in 10 mM Tris–HCl buffer (pH 7.4) and added to the respective wells at the following concentrations: vanillin, PAH, and NAC at 12.5 μg mL^{-1}; HEXNAP at 3 μg mL^{-1}; N5 and PAA at 44 μg mL^{-1}; PAANM15 at a ratio of 7.5 : 1 (94 : 12.5 μg mL^{-1}); and N5NM15, N5PAH, and PAAPAH at a ratio of 3.5 : 1 (44 : 12.5 μg mL^{-1}). Tris–HCl buffer (10 mM, pH 7.4) was added to the solvent control wells. Following another 24 h incubation at 37 °C with 5% CO_2, the spent DMEM was removed, and the MTT assay was performed as described previously (Section 2.2.3) to assess cell viability. The percentage absorbance, representing cell viability, was calculated relative to the LPS control alone (100% cell viability).

2.2.8 Cholinesterase inhibitory activity in undifferentiated SH-SY5Y cells. The inhibitory activity of the compounds against AChE and BuChE in undifferentiated SH-SY5Y cells was determined using an Ellman's assay as previously reported by Sun *et al.*,[20] with minor modifications. 10 000 Undifferentiated SH-SY5Y cells (10 000 cells/100 μL per well) were seeded and allowed to attach for 24 h at 37 °C with 5% CO_2. A fixed concentration of compounds (based on cell viability results) and the positive control, NAC, were prepared in serum-free media from stock solutions in 10 mM Tris–HCl buffer (pH 7.4). The final concentrations used were as follows: vanillin and NAC

at 12.5 μg mL^{-1}; HEXNAP at 3 μg mL^{-1}; N5 and PAA at 44 μg mL^{-1}; PAANM15 at a ratio of 7.5 : 1 (94 : 12.5 μg mL^{-1}); and N5NM15, N5PAH, and PAAPAH at a ratio of 3.5 : 1 (44 : 12.5 μg mL^{-1}). All compounds were added to the corresponding wells (100 μL per well in 6 technical replicates) after the media was removed from the wells. Tris–HCl buffer (10 mM, pH 7.4) in serum-free media was added to the negative control wells. The plate was then incubated for an additional 24 h at 37 °C with 5% CO_2. After incubation, 125 μL of DTNB solution and 25 μL of AChEI or BuChEI solution were added to each well. Absorbance was measured every 10 min at 37 °C for 80 min at 405 nm using a BioTek Synergy HT microplate reader. A calibration curve of absorbance over time was plotted for each compound, and the slope was compared to that of the negative control. Results were expressed as relative AChE and BuChE activity.

2.2.9 Amyloid-beta aggregation inhibition: ThT assay. The inhibitory activity of the compounds against amyloid-beta (Aβ) aggregation was determined using Thioflavin T (ThT) assay as previously reported by Ortega *et al.*,[21] with minor modifications testing. A 10 mM stock solution of amyloid peptide ($A\beta_{1-42}$) was prepared in DMSO and then diluted to a working concentration of 100 μM in DMSO before use. ThT was similarly prepared as a 10 mM stock solution in DMSO and diluted to 100 μM in 10 mM Tris–HCl buffer (pH 7.4). A fixed concentration of compounds (based on cell viability results), and the positive control NAC, were prepared from stock solutions in Tris–HCl buffer (10 mM, pH 7.4). The final concentrations of the compounds were as follows: NAC at 12.5 μg mL^{-1}, PAA at 44 μg mL^{-1}, and N5NM15 at a 3.5 : 1 (44 : 12.5 μg mL^{-1}) ratio. For the assay, 10 μL of each compound was added to a black-walled 96-well plate, along with 70 μL Tris–HCl buffer (10 mM, pH 7.4), 10 μL $A\beta_{1-42}$, and 10 μL ThT. Tris–HCl buffer (10 mM, pH 7.4) was added to the $A\beta_{1-42}$ control and a ThT control (without peptide or compound) was also included, with the corresponding volumes replaced by Tris–HCl buffer (10 mM, pH 7.4) and DMSO. The plate was incubated in the dark at 37 °C for 24 h. The fluorescence was measured at 446 nm excitation and 490 nm emission (BioTek Synergy HT microplate reader). The ThT control readings were subtracted from each well before analysis to account for background fluorescence. Results were expressed as the percentage of amyloid aggregation, with normalized fluorescence readings for each compound compared to the $A\beta_{1-42}$ control.

2.2.10 Transmission electron microscopy. The sample preparation for the TEM assay followed the same procedure as the ThT assay. A 10 μL sample was deposited onto a carbon-coated copper grid and left for 5 min. The grid was then stained with 1% phosphotungstic acid (10 μL) for 5 min. After removing the excess stain and allowing the sample to dry, it was transferred for imaging using a JEOL1400Plus TEM (JEOL, Japan).

2.3 Statistical analysis

Results are presented as mean ±SD or SEM (with at least 3 technical replicates) from three independent experiments (n = 3) unless otherwise stated. Statistical analysis was performed using both Microsoft Excel 2019 and GraphPad Prism 10 (GraphPad Software, USA), and a significant difference was determined using the one-way ANOVA and Dunnett's multiple comparisons tests ($^{*}p < 0.05$, $^{**}p < 0.01$, $^{***}p < 0.001$ $^{****}p < 0.0001$, ns denotes not significant).

3. Results and discussion

3.1 Development, characterisation, and cytotoxicity of nano-polyplexes

A novel strategy for developing a multi-target treatment for NDs involves developing a PEC between two distinct PDCs with opposite charges. This approach facilitates the formation of nano-polyplexes, which may enhance drug delivery and therapeutic efficacy.[3]

To aid clarity, the polymers, conjugates, and nano-polyplex systems used in this study are summarised in Table 1. The following systems were prepared and studied: NM15, N5, PAAPAH, PAANM15, N5PAH and N5NM15.

Prior to developing nano-polyplexes, cytotoxicity was determined for the two lead conjugates, NM15 and N5, using the MTT assay. The colorimetric MTT assay measures cellular metabolic activity by assessing the conversion of MTT into purple formazan crystals by mitochondrial dehydrogenases in viable cells.[22] This study aimed to determine the concentrations at which N5 and NM15 are non-toxic to undifferentiated SH-SY5Y and BV-2 cells. Undifferentiated SH-SY5Y cells were chosen as they are widely used neuronal models for studying neurotoxicity, AD mechanisms, and pathways involving Aβ and OS.[23] BV-2 cells were selected for their relevance in studying

Table 1 Summary of polymers, conjugates, and nano-polyplex formulations used in this study

Name/acronym	Components	Type	Description
PAA	Polyacrylic acid	Polymer	Anionic polymer backbone
PAH	Polyallylamine hydrochloride	Polymer	Cationic polymer backbone
NM15	PAH + Vanillin	Polymer–drug conjugate	Conjugate of polyallylamine with vanillin
N5	PAA + Naphthalimidohexylamine	Polymer–drug conjugate	Conjugate of polyacrylic acid with naphthalimidohexylamine
PAAPAH	PAA + PAH	Blank nano-polyplex	Electrostatic polyplex of unmodified polymers (control)
PAANM15	PAA + NM15	PAANM15 nano-polyplex	Electrostatic polyplex of PAA and NM15
N5PAH	N5 + PAA	N5PAH nano-polyplex	Electrostatic polyplex of N5 and PAH
N5NM15	N5 + NM15	N5NM15 Nano-polyplex	Final drug-loaded nano-polyplex formed by electrostatic interaction of two drug-conjugated polymers

inflammatory pathways, providing insights into the role of neuroinflammation in NDs.[23]

Before proceeding with the conjugates, the MTT assay was performed on Tris–HCl buffer at pH 7.4 at different concentrations in undifferentiated SH-SY5Y and BV-2 cells, as this buffer was used to prepare the conjugates and nano-polyplexes. Based on the results, 10 mM Tris–HCl pH 7.4 was selected as the optimal buffer concentration to prepare all the stock solutions of the conjugates and nano-polyplexes (Fig. S3, ESI†). Results indicated that NM15 was significantly ($p \leq 0.0001$) toxic against undifferentiated SH-SY5Y cells at all tested concentrations ranging, from 8–1000 μg mL^{-1} (Fig. 2). The observed toxicity of NM15 was attributed to the positive charge on the polymer polyallylamine hydrochloride (PAH).[24–26] Various studies[27,28] have combined anionic polymers with cationic micelles for gene delivery (positive surface charges of cationic polymers bind to negatively charged nucleic acids (DNA or RNA) *via* electrostatic interactions) to partially shield the positively charged surfaces of these micelles. This strategy effectively reduces toxicity while maintaining moderate transfection efficiencies. Therefore, to reduce the toxicity of NM15, the PEC of NM15 was developed by adding NM15 to an anionic polymer, polyacrylic acid (PAA), to partially shield the cationic charge of the conjugates, resulting in the development of PAANM15 nano-polyplexes. PAA was used in excess relative to NM15, which was based on preliminary cytotoxicity studies, where NM15 displayed notable toxicity in SH-SY5Y cells even at low concentrations (Fig. 2). Increasing the concentration of NM15 while keeping PAA constant would have elevated the overall toxicity of the PAANM15 formulation. PAANM15 was characterized using a Zetasizer to ensure a uniform particle size (Table 2). The Zetasizer analysis also provided measurements of the polydispersity index (PDI). PDI represents the distribution of particle sizes within a sample, with values ranging from

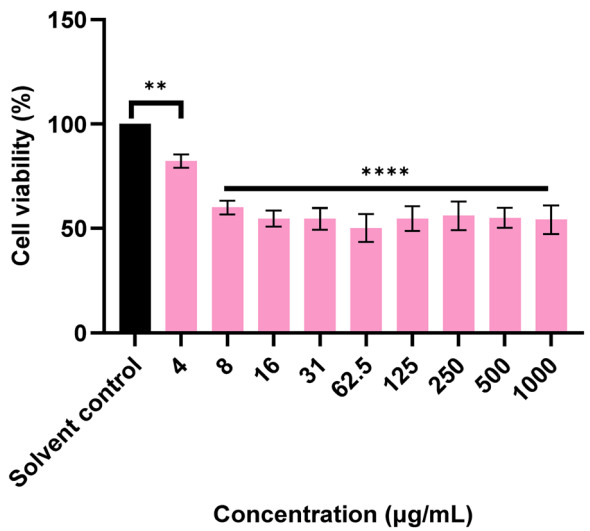

Fig. 2 Cell viability of NM15 in undifferentiated SH-SY5Y cells determined using an MTT assay after 24 h of treatment. Data presented as mean ± SEM (n = 3 independent experiments), significant difference *via* one-way ANOVA (****$p \leq 0.0001$), and Dunnett's multiple comparisons tests.

Table 2 Particle size analysis of PAANM15 at room temperature (20 °C ± 2 °C). Data presented as mean ±SD (n = 3)

PAANM15 at different mass ratio	Concentration (μg mL^{-1})	Particle size (nm)	PDI
1 : 1	25 : 25	417 ± 154	0.27 ± 0.10
5 : 1	125 : 25	69.5 ± 16.0	0.49 ± 0.13
7.5 : 1	188 : 25	33.5 ± 4.10	0.26 ± 0.08
10 : 1	250 : 25	54.6 ± 5.10	0.35 ± 0.06

0.0, indicating a monodisperse sample, to 1.0, indicating a highly polydisperse. A PDI value of 0.3 or below typically indicates a relatively uniform or monodisperse formulation.[29]

The PAANM15 nano-polyplexes, at different ratios, exhibited particle sizes below 100 nm, except for the 1 : 1 ratio, which had particle sizes greater than 400 nm (Table 2). All ratios produced clear solutions, except for the 1 : 1 ratio, which resulted in a translucent solution (Fig. S4, ESI†). The translucency observed at the 1 : 1 ratio is likely due to incomplete or non-stoichiometric charge interactions, leading to less efficient complexation and the formation of larger particles.[30] Based on the data in Table 2, the 7.5 : 1 ratio was selected as it produced the smallest particle sizes with a PDI below 0.3. Additionally, a short-term stability study was conducted over 7 days at room temperature for PAANM15 and PAAPAH (polyacrylic acid–polyallylamine hydrochloride) nano-polyplexes at three different concentrations on the selected ratio of 7.5 : 1 (Table 3).

The results from Table 3 indicated that both PAANM15 and PAAPAH nano-polyplexes exhibited particle sizes of less than 100 nm and demonstrated stability over 7 days stored at room temperature. This is evident as the particle sizes and PDIs remained stable with no significant changes observed ($p > 0.05$). The Zetasizer analysis also provided zeta potential measurements of the PEC. Zeta potential, which measures the degree of repulsion between charged particles in a dispersion, plays a key role in maintaining stability. A zeta potential, around ±30 mV, helps to prevent particle aggregation by promoting strong repulsion between particles. The zeta potential also governs charge interactions within the formulation.[31] The analysis revealed that both PAANM15 and PAAPAH possess a negative charge, indicating that the anionic polymer PAA effectively shields the cationic charge of the NM15 conjugate, contributing to the overall stability of the complex. The consistently negative zeta potential values for both PAANM15 and PAAPAH suggest that they form stable colloidal dispersions.

The cytotoxicity of PAANM15 and other starting materials showed that PAANM15 maintained cell viability above 90%, confirming that the nano-polyplex was non-toxic in either cell line at a ratio of 7.5 : 1 (188 : 25 μg mL^{-1} for undifferentiated SH-SY5Y and 375 : 50 μg mL^{-1} for BV-2 cells (as BV-2 cells contains both adherent and floating cells), with both cells lines had a final concentration of 94 : 12.5 μg mL^{-1}) (Fig. 3).

Similarly, the cell viability study was conducted on undifferentiated SH-SY5Y and BV-2 cells treated with anticholinesterase

Table 3 Particle size analysis and stability of PAANM15 and PAAPAH stored at room temperature (20 °C ± 2 °C). Data presented as mean ±SD (n = 3)

Compounds	Day	Concentration (μg mL^{-1})	Particle size (nm)	PDI	Zeta potential (mV)
PAANM15	Day 1	188 : 25	33.5 ± 4.10	0.26 ± 0.08	−25.0 ± 1.90
		375 : 50	44.8 ± 2.60	0.23 ± 0.01	−36.6 ± 3.40
		750 : 100	77.2 ± 14.0	0.20 ± 0.01	−29.2 ± 1.60
PAAPAH		188 : 25	34.5 ± 4.30	0.31 ± 0.05	−30.9 ± 5.80
		375 : 50	45.9 ± 3.80	0.22 ± 0.02	−37.0 ± 2.40
		750 : 100	72.9 ± 1.40	0.18 ± 0.04	−33.5 ± 2.00
PAANM15	Day 2	188 : 25	34.2 ± 4.40	0.28 ± 0.05	−27.0 ± 4.00
		375 : 50	44.7 ± 4.20	0.20 ± 0.04	−35.1 ± 2.30
		750 : 100	76.7 ± 15.0	0.19 ± 0.01	−30.1 ± 1.20
PAAPAH		188 : 25	31.3 ± 2.50	0.26 ± 0.06	−26.0 ± 3.30
		375 : 50	44.7 ± 4.50	0.20 ± 0.03	−36.6 ± 1.60
		750 : 100	72.2 ± 0.70	0.17 ± 0.03	−32.7 ± 1.70
PAANM15	Day 7	188 : 25	38.6 ± 8.10	0.30 ± 0.06	—
		375 : 50	43.7 ± 2.70	0.20 ± 0.02	—
		750 : 100	76.5 ± 14.0	0.20 ± 0.01	—
PAAPAH		188 : 25	35.3 ± 3.00	0.31 ± 0.03	—
		375 : 50	44.3 ± 4.60	0.19 ± 0.03	—
		750 : 100	69.8 ± 1.70	0.18 ± 0.04	—

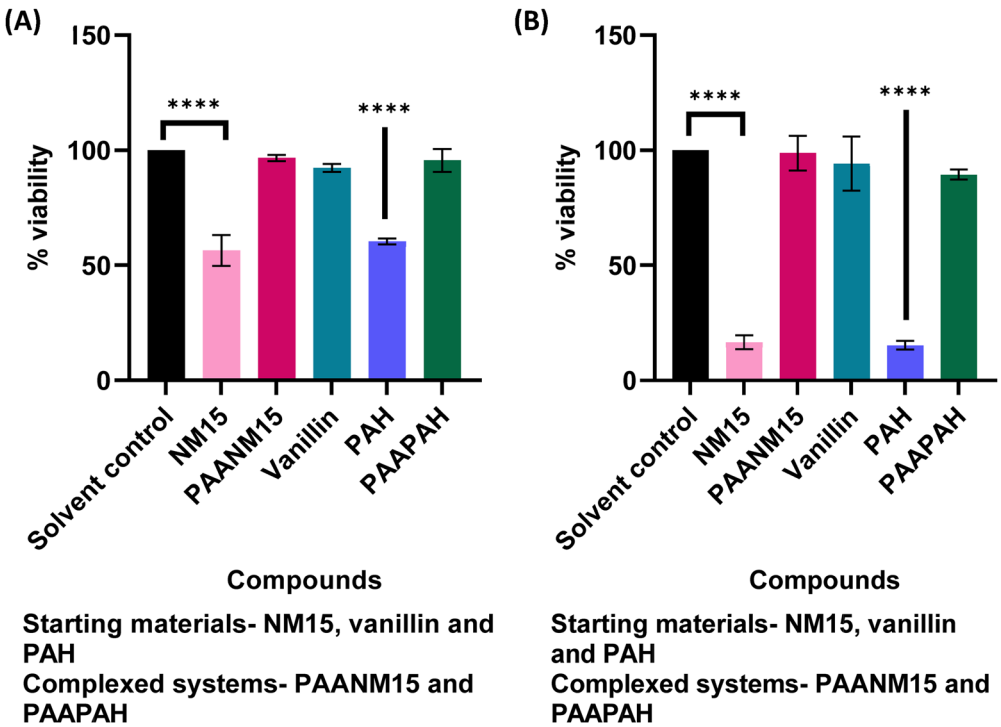

Fig. 3 Cell viability of PAANM15 and the starting materials in (A) undifferentiated SH-SY5Y and (B) BV-2 cell lines determined using an MTT assay after 24 h of treatment. Data presented as mean ± SEM (n = 3 independent experiments), significant difference *via* one-way ANOVA (****$p \leq 0.0001$), and Dunnett's multiple comparisons tests. The final concentrations used were as follows: NM15, vanillin, and PAH at 12.5 μg mL^{-1}; PAANM15 and PAAPAH at a ratio of 7.5 : 1 with a final concentration of 94 : 12.5 μg mL^{-1}.

conjugate N5, and the results showed that N5 was non-toxic to undifferentiated SH-SY5Y cells at concentrations up to 250 μg mL^{-1} (Fig. 4(A)). However, N5 exhibited significant toxicity ($p \leq 0.0001$) at concentrations from 125 μg mL^{-1} in BV-2 cells (Fig. 4(B)). The cell viability study was also conducted on undifferentiated SH-SY5Y and BV-2 cells treated with HEXNAP (Fig. S5, ESI†).

This outcome was expected due to the use of different cell lines. BV-2 cells are murine microglial cells, derived from v-raf/v-myc-immortalized murine neonatal microglia, which are small and round in shape, often becoming amoeboid when activated,[32] making them more susceptible to toxic effects. In contrast, undifferentiated SH-SY5Y cells are human neuroblastoma cells, derived from the thrice-cloned parental SK-N-SH cell line, originally from a metastatic bone tumour, and are densely packed and proliferative, resembling immature catecholaminergic neuroblasts.[33] These cytotoxicity studies provided a baseline concentration range for NM15 and N5,

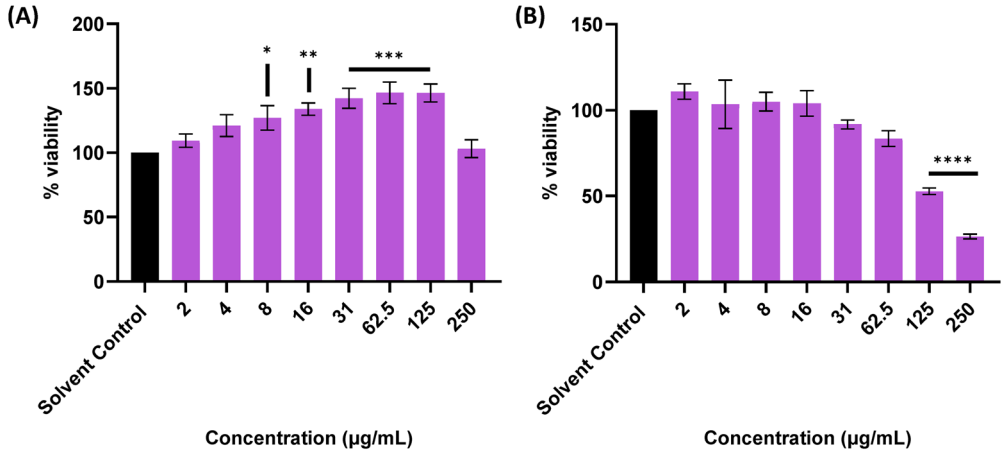

Fig. 4 Cell viability of N5 in (A) undifferentiated SH-SY5Y and (B) BV-2 cell lines determined using an MTT assay after 24 h of treatment. Data presented as mean ± SEM (n = 3 independent experiments), significant difference *via* one-way ANOVA (****$p \leq 0.0001$), and Dunnett's multiple comparisons tests.

which was used to develop a non-toxic lead nano-polyplex (N5NM15).

From this point onward, the focus of the development and characterisation studies was to identify the optimal mass ratio and evaluate the toxicity of the lead nano-polyplex (N5NM15), along with the N5PAH and PAAPAH control systems at the same ratio. The lead nano-polyplex (N5NM15) was developed by gradually mixing a fixed concentration of NM15 with varying mass of N5, at pH 7.4 to produce a stable nano-polyplex. N5 was used in excess relative to NM15, which was based on preliminary NM15 cytotoxicity studies (Fig. 2) as discussed earlier. The successful formation of the nano-polyplex was confirmed by Zetasizer analysis (Table 4).

The results from Table 4 indicated that the smallest and most uniform particles were observed at the 2 : 1 ratio, making this the most stable formulation in terms of size and distribution. However, as the ratio of N5 increased (3.5 : 1, 5 : 1, and 7.5 : 1), larger particle sizes were observed. The higher PDI indicates a broader size distribution within the particle population, suggesting that the particles are polydisperse. This could be attributed to the structural properties of the naphthalimido moiety in N5. While π–π interactions between the aromatic rings of the naphthalimido group and vanillin in NM15 are expected to contribute to the formation of compact complexes, the flexibility of the linker chain and polymer backbones likely hinders the ability of the naphthalimido group to orient itself effectively around the vanillin. This reduced efficiency of interaction results in larger and less uniform particle sizes. To determine the optimal N5NM15 ratio, a cell viability study was conducted in undifferentiated SH-SY5Y and BV-2 cell lines (Fig. 5). The results showed that none of the ratios were toxic in undifferentiated SH-SY5Y cells (Fig. 5(A)). However, all ratios exhibited significant toxicity ($p \leq 0.0001$) in BV-2 cells (Fig. 5(B)). Amongst the tested ratios, the 3.5 : 1 ratio was selected as the lead nano-polyplex because it demonstrated higher cell viability (>75%, $p \leq 0.001$) in BV-2 cells compared to the other ratios. Additionally, both N5PAH and PAAPAH nano-polyplexes (3.5 : 1 ratio) were non-toxic in undifferentiated SH-SY5Y cells (Fig. 5(C)) but showed significant toxicity in BV-2 cells (Fig. 5(D)).

Additionally, a short-term stability study was conducted over 7 days at room temperature on the N5NM15, N5PAH, and PAAPAH nano-polyplexes at two different concentrations on the selected ratio of 3.5 : 1 (Table 5).

The results revealed that both N5NM15 and N5PAH nano-polyplexes exhibited a larger particle size compared to PAAPAH (Table 5). This is likely due to the presence of the aromatic rings of the naphthalimido group in N5, which is more hydrophobic than PAA. The presence of hydrophobic N5 encourages the formation of micelles, where the hydrophobic cores are surrounded by the more hydrophilic NM15 or PAH, leading to a larger overall particle size in the N5NM15 and N5PAH nano-polyplexes. Additionally, steric hindrance likely results in a more diffuse and polydisperse particle population. Interestingly, the particle size at lower concentrations of N5NM15 and N5PAH decreased significantly over 7 days ($p \leq 0.001$), suggesting that the particles become more compact over time. This observation may indicate that the nano-polyplex takes a longer period to reach equilibrium. The observed reduction in nano-polyplex size over time can also be influenced by ionic interactions due to the Tris–HCl buffer. The buffer's ions may interfere with the electrostatic interactions between the N5 and NM15, leading to a more compact structure and smaller particle size, suggesting they may have initially formed fewer compact structures. To address this, further exploration of charge balance and N5 and NM15 conjugate ratios is essential.

Table 4 Particle size analysis of N5NM15 at room temperature (20 °C ± 2 °C). Data presented as mean ±SD (n = 3)

N5NM15 at different mass ratio	Concentration (μg mL^{-1})	Particle size (nm)	PDI
2 : 1	50 : 25	76.7 ± 4.20	0.38 ± 0.02
3.5 : 1	87.5 : 25	186 ± 18	0.57 ± 0.06
5 : 1	125 : 25	124 ± 6.10	0.60 ± 0.13
7.5 : 1	187.5 : 25	176 ± 9.40	0.59 ± 0.03

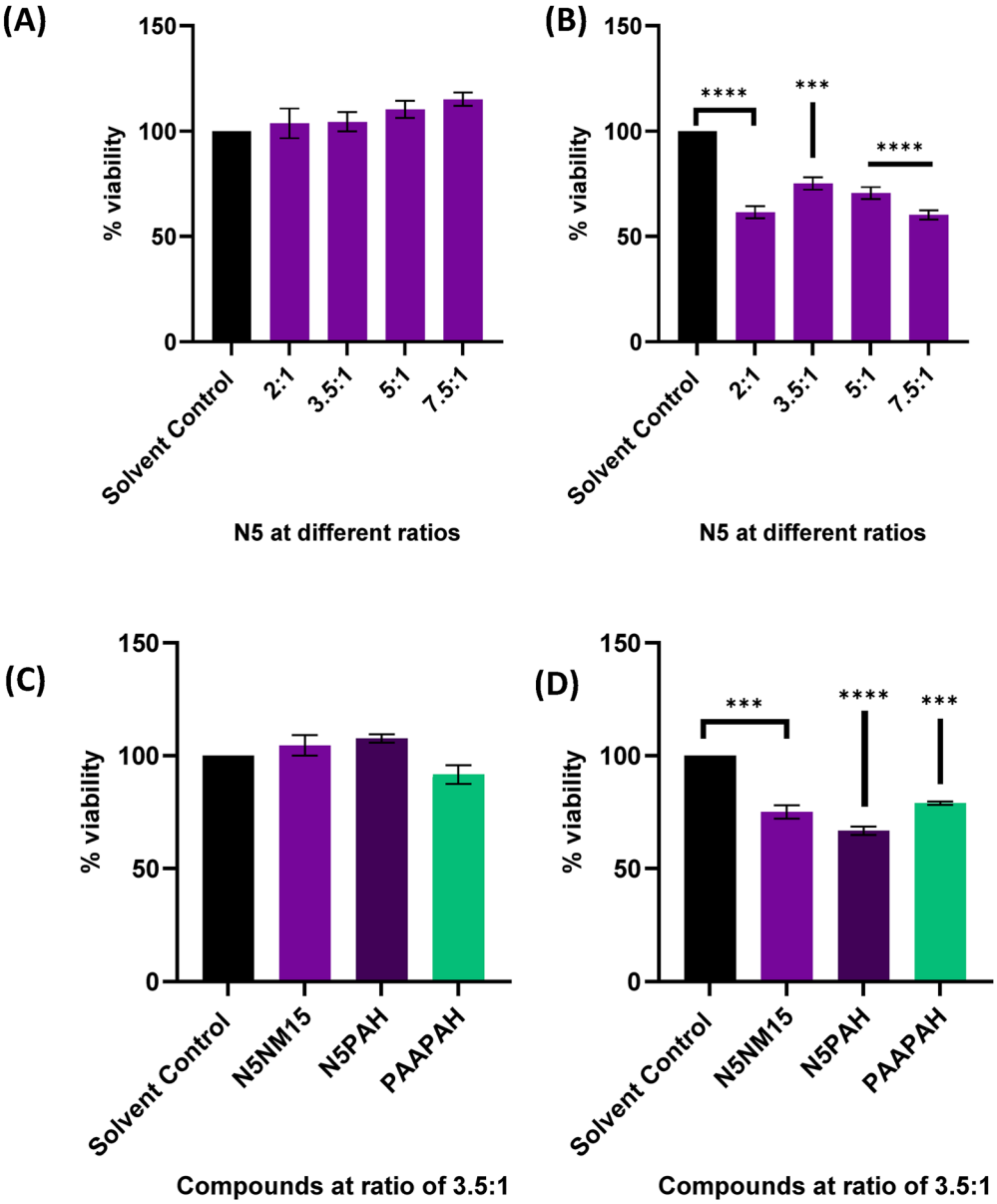

Fig. 5 Cell viability of N5NM15 and starting materials in (A) and (C) undifferentiated SH-SY5Y and (B) and (D) BV-2 cell lines determined using an MTT assay after 24 h of treatment. Data presented as mean ± SEM (n = 3 independent experiments), significant difference *via* one-way ANOVA (****$p \leq 0.0001$ for BV-2), and Dunnett's multiple comparisons tests. The final concentrations used were as follows: 2 : 1 (25 : 12.5 μg mL^{-1}), 3.5 : 1 (44 : 12.5 μg mL^{-1}), 5 : 1 (62.5 : 12.5 μg mL^{-1}), 7.5 : 1 (94 : 12.5 μg mL^{-1}); N5NM15, N5PAH, and PAAPAH at a ratio of 3.5 : 1 with a final concentration of 44 : 12.5 μg mL^{-1}.

Additionally, investigating the impact of varying buffer conditions, such as ionic strength, could provide insights into environmental effects on particle stability. Furthermore, the N5NM15 demonstrated excellent stability, as indicated by its zeta potential, which was lower than −45 mV. Overall, over time, all nano-polyplexes maintained relatively consistent particle sizes and zeta potential, suggesting good colloidal stability. These data indicate that the N5NM15 nano-polyplex is a promising candidate for further studies due to its smaller particle size, stability, and potential for forming micellar structures, which could enhance drug delivery.

While the stability of the nano-polyplex was confirmed over time in Tris–HCl buffer (pH 7.4, 10 mM) using DLS and zeta potential analysis; however, these conditions do not fully replicate the complexity of biological environments. In media such as plasma or cell culture medium, the presence of proteins, salts, and other biomolecules can interfere with DLS measurements, making Zetasizer analysis unreliable due to non-specific scattering and potential protein-induced aggregation.[34] To accurately assess nano-polyplex stability under such conditions, an alternative approach such as asymmetric flow field-flow fractionation (AF4) coupled with multi-

Table 5 Particle size analysis and stability study of N5NM15, N5PAH, and PAAPAH stored at room temperature (20 °C ± 2 °C). Data presented as mean ±SD (n = 3), significant difference *via* one-way ANOVA (***$p \leq 0.001$ for N5NM15 and N5PAH, *$p \leq 0.05$ for PAAPAH), and Dunnett's multiple comparisons tests

Compounds	Day	Concentration (μg mL^{-1})	Particle size (nm)	PDI	Zeta potential (mV)
N5NM15	Day 1	87.5 : 25	186 ± 18.0	0.57 ± 0.06	−49.8 ± 3.90
		175 : 50	126 ± 12.0	0.59 ± 0.04	−53.8 ± 2.90
N5PAH		87.5 : 25	214 ± 23.0	0.52 ± 0.06	−45 ± 1.70
		175 : 50	174 ± 8.2.0	0.62 ± 0.02	−46.3 ± 2.20
PAAPAH		87.5 : 25	29.6 ± 3.90	0.24 ± 0.06	−15.9 ± 2.90
		175 : 50	37.8 ± 2.70	0.19 ± 0.06	−30.9 ± 2.80
N5NM15	Day 2	87.5 : 25	142 ± 7.70**	0.60 ± 0.04	−48.8 ± 2.30
		175 : 50	124 ± 8.70	0.56 ± 0.03	−54.2 ± 2.80
N5PAH		87.5 : 25	198 ± 17.0	0.49 ± 0.07	−41 ± 2.50
		175 : 50	182 ± 10.0	0.52 ± 0.08	−54.2 ± 2.80
PAAPAH		87.5 : 25	38.0 ± 7.50	0.45 ± 0.07	−27.3 ± 3.70
		175 : 50	43.8 ± 1.40	0.35 ± 0.02	−30.3 ± 2.40
N5NM15	Day 7	87.5 : 25	102 ± 4.80***	0.58 ± 0.03	—
		175 : 50	113 ± 5.60	0.52 ± 0.03	—
N5PAH		87.5 : 25	118 ± 6.80**	0.63 ± 0.03	—
		175 : 50	165 ± 15.0	0.53 ± 0.05	—
PAAPAH		87.5 : 25	37.0 ± 8.10	0.42 ± 0.02	—
		175 : 50	46.7 ± 4.80*	0.39 ± 0.01	—

angle light scattering (MALS) is more suitable, as they allow separation and characterisation of intact nanoparticles in complex biological environments.[35,36] Future work will focus on optimising this technique to evaluate nano-polyplex behaviour in biologically relevant media.

The particle size and morphology of the N5NM15 and N5PAH nano-polyplexes were further confirmed using cryo-TEM (Fig. 6). For accurate visualization, a high concentration of nano-polyplexes (ratio 3.5 : 1–700 : 200 μg mL^{-1}) was prepared. The results revealed that the N5NM15 and N5PAH nano-polyplexes had particle sizes of approximately 30.5 ± 7.9 nm and 34.9 ± 5.3 nm, respectively, with predominantly spherical to oval shapes (Fig. 6(A) and (B)). In contrast, when the same concentration of N5NM15 and N5PAH nano-polyplexes was analysed using a Zetasizer, the observed particle sizes were 107.4 ± 1.80 nm and 144.2 ± 25.0 nm, with PDI values of 0.26 ± 0.02 and 0.52 ± 0.04, and zeta potentials of −61.8 ± 3.20 mV and −51.5 ± 2.40 mV, respectively. The observed difference in particle size between cryo-TEM and DLS is typically attributed to the polyelectrolyte complexes, which possess strong electrostatic interactions due to the presence of charged groups. These charged particles are surrounded by a dynamic electrical double layer, comprising a Stern layer and a diffuse layer, which moves with the particle during Brownian motion, thereby increasing the apparent hydrodynamic diameter measured by DLS.[37] However, cryo-TEM directly visualizes the actual physical size of the particles without the influence of the surrounding solvent, resulting in a smaller measured size.[38] Therefore, the larger size observed by DLS compared to cryo-TEM is a common phenomenon for polyelectrolyte complexes. Similar discrepancies between cryo-TEM and DLS measurements have been frequently reported in the literature, especially for hydrophilic or polymer-coated nanoparticles.[39,40] For example, Sarkar and Ghosh[40] reported that folic acid–PEG–hyaluronic acid–curcumin nanoparticles exhibited a DLS size of 120.6 ± 2.2 nm, while the corresponding TEM images showed a much smaller core size of 35.2 ± 3.6 nm. This is attributed to the hydrophilic coating on the nanoparticle surface, which increases the hydrodynamic diameter in aqueous environments. Therefore, cryo-TEM is considered a gold standard technique for measuring particle size. cryo-TEM was not performed on PAANM15 or PAAPAH as these systems did not form well-defined micelles due to the lower hydrophobicity of NM15, and the resulting particles were too small for meaningful imaging.

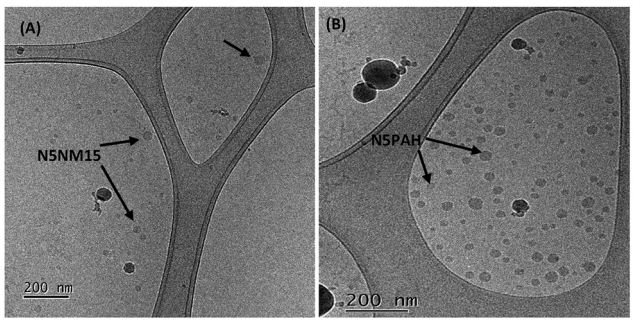

Fig. 6 Cryo-TEM image of (A) N5NM15 and (B) N5PAH nano-polyplexes (scale bar = 200 nm).

The observed difference in particle size between cryo-TEM and DLS is typically attributed to the polyelectrolyte complexes, which possess strong electrostatic interactions due to the presence of charged groups. These charged particles are surrounded by a dynamic electrical double layer, comprising a Stern layer and a diffuse layer, which moves with the particle during Brownian motion, thereby increasing the apparent hydrodynamic diameter measured by DLS. However, cryo-TEM directly visualizes the actual physical size of the particles without the influence of the surrounding solvent, resulting in a smaller measured size.[38] Therefore, the larger size observed by DLS compared to cryo-TEM is a common phenomenon for polyelectrolyte complexes.

While the formulation of the N5NM15 nano-polyplex was supported by changes in particle size, PDI, and zeta potential, these measurements provide indirect evidence of complex formation. The presence of free unreacted polymer, non-stoichiometric assemblies, or incomplete complexation cannot be ruled out solely on the basis of cryo-TEM, DLS, and zeta potential data. To confirm the nature of the nano-polyplex whether it forms a stoichiometric insoluble complex, a stable non-stoichiometric system, or contains free polymers, further characterisation techniques such as multi-angle DLS and size-exclusion chromatography (SEC) are required. These methods will help distinguish the nano-polyplex from its individual polymer components and provide a more comprehensive understanding of the system.

Overall, the lead N5NM15 nano-polyplex was successfully developed and characterised. Further analysis was conducted to determine whether it possesses antioxidant and cholinesterase inhibitory activities.

3.2 *In vitro* antioxidant activity of N5NM15 nano-polyplex: ORAC assay

The antioxidant activity of nano-polyplexes (PAANM15 and N5NM15), NM15, and vanillin were determined using the oxygen radical absorbance capacity (ORAC) assay. This assay works under the mechanism of hydrogen atom transfer (HAT), by measuring the ability of antioxidants to inhibit oxidation induced by peroxyl radicals.[41] The ORAC assay is biologically relevant compared to other antioxidant assays, such as 2,2-diphenyl-1-picrylhydrazyl (DPPH) and ferric reducing antioxidant power (FRAP), because it mimics *in vivo* conditions by using peroxyl radicals, the most prevalent free radicals that predominate in lipid oxidation in biological systems.[41] This makes the ORAC assay particularly suited for assessing antioxidant potential in a manner that closely reflects physiological OS conditions. The results obtained for the ORAC assay performed on the nano-polyplexes are presented in Fig. 7.

NM15 and the nano-polyplexes exhibited significantly lower antioxidant activity ($p < 0.0001$) compared to vanillin (6553 ± 482 μmolTE/1 g) (Fig. 7(A)). However, based on elemental analysis % attachment data from our previous study,[13] it was determined that 17.8% of vanillin was attached in the NM15 conjugate. Thus, the adjusted NM15 and N5NM15 nano-polyplex showed significantly enhanced antioxidant activity compared to vanillin ($p < 0.001$, Fig. 7(B)). The presence of the HC═N linkage within the NM15 conjugate (Fig. 1(A)) plays a crucial role in augmenting the antioxidant activity of both the conjugate and the nano-polyplexes.[13] Additionally, there was no significant difference in antioxidant activity between the NM15 conjugate and the nano-polyplexes, suggesting that the activity is maintained after the development of the nano-polyplex. HEXNAP, N5, N5PAH, PAAPAH, PAA, and PAH showed no antioxidant activity (data not shown). This finding is novel, as no previous work has been reported on developing nano-polyplexes between two PDCs and determining their antioxidant activity.

3.3 *In vitro* cholinesterase inhibitory activity of N5NM15 nano-polyplex: Ellman's assay

In AD, the levels of the neurotransmitter acetylcholine (ACh) are hydrolysed by AChE and BuChE, leading to memory,

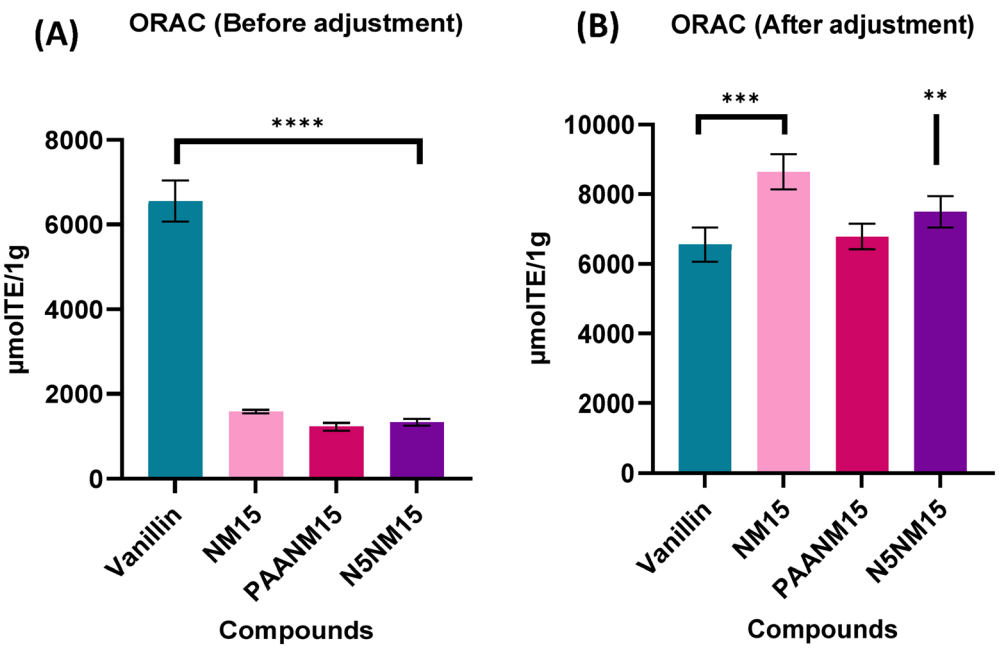

Fig. 7 Antioxidant activity of N5NM15 nano-polyplex (A) before adjustment and (B) after adjustment. Data presented as mean ±SD (n = 3), significant difference *via* one-way ANOVA (****$p \leq 0.0001$ before adjustment, ***$p \leq 0.001$ after adjustment), and Dunnett's multiple comparisons tests. The final concentrations used were as follows: vanillin and NM15 at 12.5 μg mL^{-1}; PAANM15 at a ratio of 7.5 : 1 with a final concentration of 94 : 12.5 μg mL^{-1}; N5NM15, at a ratio of 3.5 : 1 with a final concentration of 44 : 12.5 μg mL^{-1}.

cognitive decline, and behavioral disorders.[42] Therefore, inhibiting these enzymes can help prevent the breakdown of ACh, thereby increasing its levels and potentially improving neurotransmission in AD patients.[42]

The cholinesterase inhibitory activity of N5NM15 and N5PAH nano-polyplexes was evaluated using Ellman's assay, which measures enzyme activity by hydrolyzing the substrates acetylthiocholine iodide (AChEI) or butyrylthiocholine iodide (BuChEI) through AChE or BuChE, respectively. Fig. 8 shows the evaluation of these nano-polyplexes against AChE and BuChE enzymes.

Both N5NM15 and N5PAH demonstrated significantly lower activity ($p < 0.0001$) compared to HEXNAP (Fig. 8(A) and (B)). However, based on the elemental analysis percentage attachment data from our previous study,[13] it was determined that 1.04% of HEXNAP was attached to the N5 conjugate. Thus, the adjusted nano-polyplexes exhibited significantly enhanced cholinesterase inhibitory activity compared to HEXNAP ($p < 0.0001$, Fig. 8(C) and (D)).

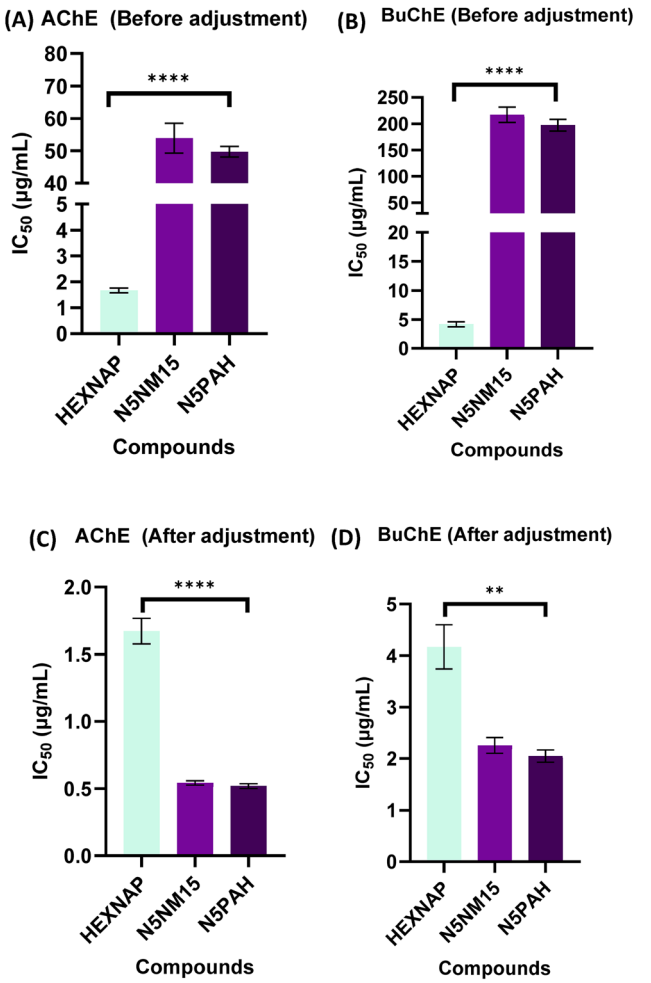

Fig. 8 Ellman's AChE and BuChE inhibitory activity of N5NM15 nano-polyplex before adjustment (A) and (B) and after adjustment (C) and (D). Data presented as mean ± SD (n = 3), significant difference *via* one-way ANOVA (****$p \leq 0.0001$ before adjustment for AChE and BuChE, ****$p \leq 0.0001$ for AChE and **$p \leq 0.01$ for BuChE after adjustment), and Dunnett's multiple comparisons tests.

Previous data[13] indicated that the cholinesterase inhibitory activity of the adjusted N5 was $IC_{50} = 0.56 \pm 0.03$ μg mL^{-1} for AChE and 0.91 ± 0.06 μg mL^{-1} for BuChE. While there was no significant difference between the AChE inhibitory activity of N5 and the nano-polyplexes, a significant difference ($p < 0.001$) was observed in the BuChE inhibitory activity between N5 and the nano-polyplexes. Nonetheless, the nano-polyplexes remained more potent than HEXNAP. Additionally, the nano-polyplexes exhibited stronger activity against AChE than BuChE, which is consistent with the previous study on N5 and HEXNAP. This increased inhibitory activity against AChE is attributed to the flexible hexyl group in HEXNAP, which plays a key role in enhancing its inhibitory effects against AChE.[9,43] Vanillin, NM15, PAANM15, PAAPAH, PAA, and PAH showed no cholinesterase inhibitory activity (data not shown).

A kinetic study was conducted to determine the type of inhibition exhibited by N5NM15 nano-polyplex. The study focused on the BuChE enzyme, as BuChE activity tends to increase whilst AChE activity decreases as AD progresses.[44] The type of BuChE inhibition exerted by N5NM15 and N5PAH was determined using Lineweaver–Burke plots. The V_{max} and K_m values were then calculated based on these plots. The results showed that N5NM15 and N5PAH nano-polyplexes competitively inhibited the BuChE enzyme, as indicated by their V_{max} and K_m values (Fig. 9(A) and (B)).

For the N5NM15 nano-polyplex, the IC_{50} value indicated a V_{max} of 0.0016 and a K_m of 1.740 mM, compared to the negative control (V_{max} of 0.0017 and a K_m of 0.5 mM). Similarly, the N5PAH nano-polyplex showed a V_{max} of 0.0015 and a K_m of 1.427 mM, while the negative control had a V_{max} of 0.0017 and a K_m of 0.495 mM. Although the V_{max} values for both nano-polyplexes did not differ significantly from the negative control, the significantly higher K_m values ($p \leq 0.01$) confirmed that they competitively inhibit the BuChE enzyme. Furthermore, a kinetic study was conducted on N5NM15 at a concentration of 44 : 12.5 μg mL^{-1}, which was used in all further studies and was based on the cell viability studies ratio of 3.5 : 1. The results are consistent with those observed at other concentrations of N5NM15, demonstrating that it competitively inhibits BuChE even at this low concentration (Fig. S6, ESI†). This finding aligns with our previous study[13] on N5 and HEXNAP, supporting the conclusion that the nano-polyplexes act as competitive inhibitors of BuChE. Overall, the N5NM15 nano-polyplex has the potential to increase ACh levels, thereby enhancing cholinergic neurotransmission and reducing cognitive decline associated with NDs.

3.4. *In vitro* cellular protective and anti-inflammatory activity

In many age-related diseases, cell death is often triggered by the presence of reactive oxygen species (ROS).[19] In this study, hydrogen peroxide (H_2O_2) was used as a stressor to induce OS in undifferentiated SH-SY5Y and BV-2 cells. H_2O_2 is a common ROS produced in cells by superoxide dismutase's as a by-product of the superoxide anion (O_2^{2-}). As a relatively stable

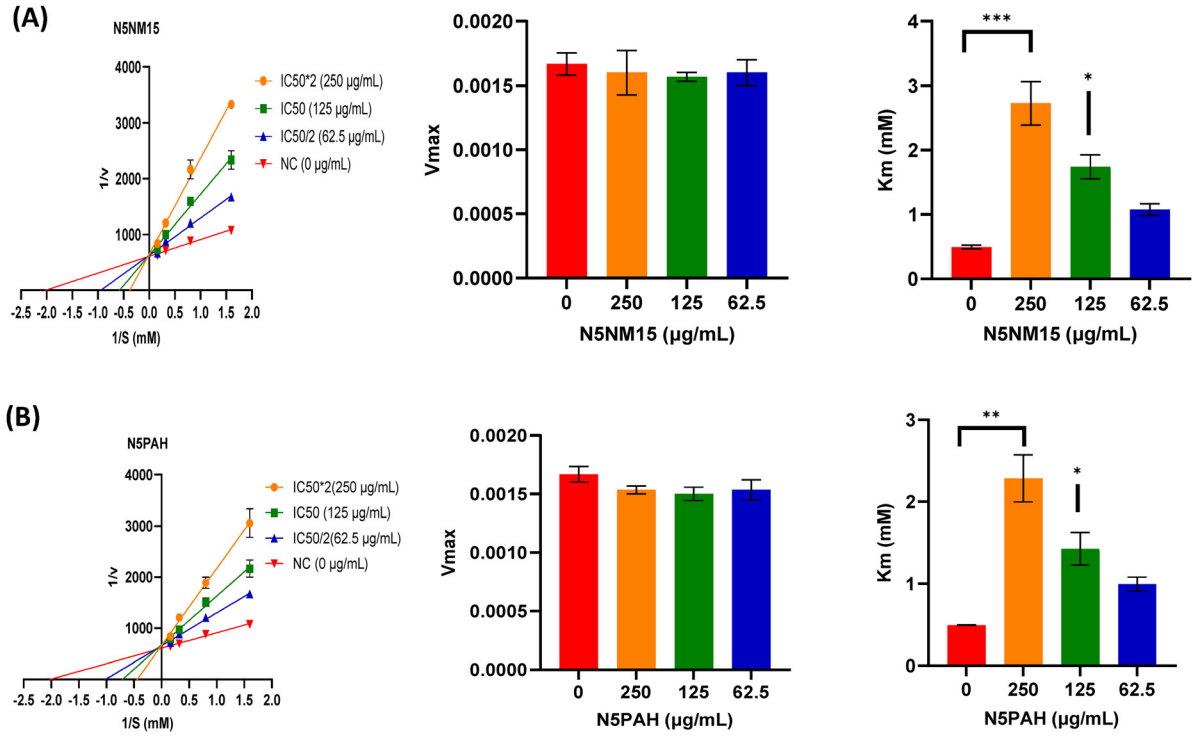

Fig. 9 Ellman's BuChE kinetic study of (A) N5NM15 and (B) N5PAH nano-polyplexes. The *x*-axis represents the concentration of N5 in the N5NM15 and N5PAH nano-polyplexes, as depicted in the V_{max} and K_m graphs. Data presented as mean ± SEM (n = 3), significant difference *via* one-way ANOVA (**$p \leq 0.01$), and Dunnett's multiple comparisons tests.

and neutrally charged molecule, H_2O_2 can easily penetrate cell membranes, which has led researchers to suggest its involvement in OS signalling.[45] The optimal concentration of H_2O_2 was determined using the MTT assay for both cell lines (Fig. S7, ESI†). The protective effects of nano-polyplexes, PDCs, and their starting materials against H_2O_2-induced OS were evaluated

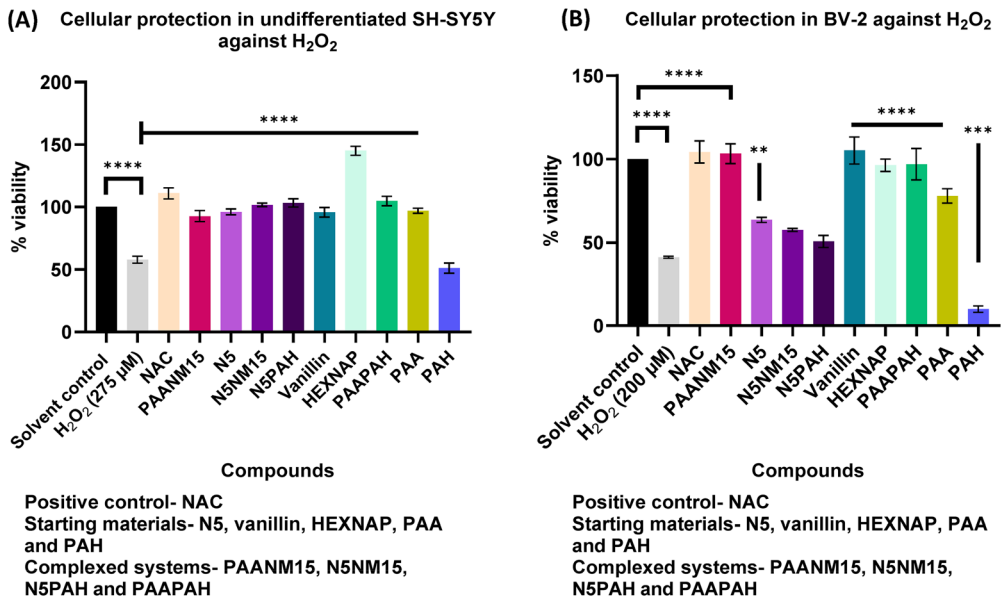

Fig. 10 Cellular protective effects of all tested compounds against H_2O_2-induced cell death in (A) undifferentiated SH-SY5Y and (B) BV-2 cells determined using an MTT assay after 24 h of treatment. Data presented as mean ± SEM (n = 3 independent experiments), significant difference *via* one-way ANOVA (****$p \leq 0.0001$), and Dunnett's multiple comparisons tests. The final concentrations used were as follows: NAC, vanillin, and PAH at 12.5 μg mL^{-1}; HEXNAP at 3 μg mL^{-1}; N5 and PAA at 44 μg mL^{-1}; PAANM15 at a ratio of 7.5 : 1 with a final concentration of 94 : 12.5 μg mL^{-1}; N5NM15, N5PAH, and PAAPAH at a ratio of 3.5 : 1 with a final concentration of 44 : 12.5 μg mL^{-1}.

using the MTT assay in both undifferentiated SH-SY5Y and BV-2 cells, with *N*-acetyl cysteine (NAC) as a positive control. NAC was chosen because of its well-documented multi-target activity in AD models and its potent protective effects, including antioxidant and anticholinesterase activities.[46,47]

Fig. 10(A) illustrates the protective effects of all tested compounds against H_2O_2-induced cell death in undifferentiated SH-SY5Y cells. All, except PAH, showed significant protective effects against OS induced by H_2O_2 ($p \leq 0.0001$). Notably, the nano-polyplex N5NM15 significantly protected SH-SY5Y cells, providing 45% protection ($p \leq 0.0001$). An important observation is that only 17.8% of vanillin and 1.04% of HEXNAP are attached to the nano-polyplexes, which highlights the higher potency of N5NM15 compared to vanillin and HEXNAP.

Fig. 10(B) illustrates the protective effects of all tested compounds against H_2O_2-induced cell death in BV-2 cells. While most compounds provided strong protection in BV-2 cells, N5NM15 and N5PAH did not exhibit significant protection in BV-2 cells, providing only 15% and 20% protection, respectively.

Additionally, microglial activation and neuroinflammation are crucial factors in the onset and progression of NDs, often occurring before the onset of conditions such as AD.[48,49] Lipopolysaccharide (LPS)-induced inflammation is widely utilised in experimental models to study neuroinflammation, given its capability to activate microglia, initiate inflammatory responses, and promote amyloid deposition.[48] The anti-inflammatory effects of nano-polyplexes, PDCs, NAC, and their respective starting materials against LPS-induced inflammation in BV-2 cells was determined using the MTT assay (Fig. 11). The optimal concentration of LPS was determined using the MTT assay (Fig. S8, ESI†). The results indicated that most compounds effectively reduced inflammation in BV-2 cells; however, N5PAH did not exhibit a significant effect in BV-2 cells, providing only a 20% reduction in inflammation. N5NM15 significantly reduced inflammation in BV-2 cells by more than 20% ($p \leq 0.05$) but, its anti-inflammatory activity was notably lower than that of other tested compounds. This reduced efficacy against H_2O_2-induced stress and LPS-induced inflammation may be attributed to a slightly toxic effect of the nano-polyplex, as discussed in Section 3.1. Such toxicity could interfere with the nano-polyplexes ability to mitigate oxidative damage and inflammation effectively, potentially due to factors such as particle size or other physicochemical properties influencing its cellular interactions.

However, PAANM15 nano-polyplex significantly protected BV-2 cells against H_2O_2-induced oxidative stress and LPS-induced inflammation ($p \leq 0.0001$), compared to N5NM15. This could be due to the PAANM15 being developed using a 7.5 : 1 ratio, resulting in smaller particle size and a lower PDI (Table 2) compared to N5NM15, which was developed using a 3.5 : 1 ratio (Table 4). Additionally, N5 was not present in PAANM15, which may contribute to the reduced toxicity observed in BV-2 cells. The different formulation likely influences the size, stability, and cellular uptake of the nano-polyplex, enhancing its ability to mitigate oxidative damage and inflammation more effectively. Therefore, further studies are required to investigate the cellular and molecular mechanisms of N5NM15 nano-polyplex in BV-2 cells, specifically focusing on their uptake, intracellular trafficking, and interactions with inflammatory and oxidative stress pathways. This will help identify key factors influencing their efficacy and toxicity, enabling optimisation for enhanced therapeutic effects.

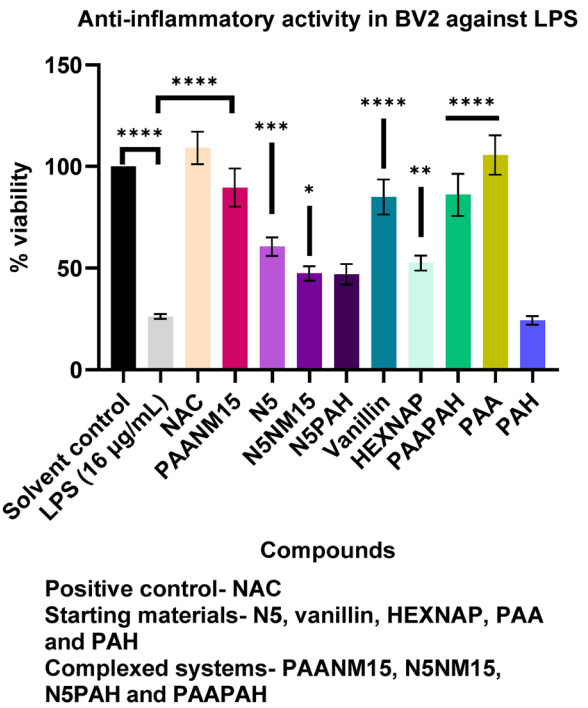

Fig. 11 Anti-inflammatory effects of all the tested compounds against LPS in BV-2 cells determined using an MTT assay after 24 h of treatment. Data presented as mean ± SEM (n = 3 independent experiments), significant difference *via* one-way ANOVA (****$p \leq 0.0001$), and Dunnett's multiple comparisons tests. The final concentrations used were as follows: NAC, vanillin, and PAH at 12.5 µg mL^{-1}; HEXNAP at 3 µg mL^{-1}; N5 and PAA at 44 µg mL^{-1}; PAANM15 at a ratio of 7.5 : 1 with a final concentration of 94 : 12.5 µg mL^{-1}; N5NM15, N5PAH, and PAAPAH at a ratio of 3.5 : 1 with a final concentration of 44 : 12.5 µg mL^{-1}.

Additionally, PAA, the anionic polymer, exhibited significant ($p \leq 0.0001$) H_2O_2-induced OS protective and anti-inflammatory effects caused by LPS in both cell lines. PAA's ability to decrease H_2O_2-induced OS suggests it may act as an effective antioxidant, while its reduction of LPS-induced inflammation indicates it could inhibit pro-inflammatory pathways in microglia. Interestingly, despite its protective effects in cell-based assays, PAA showed no antioxidant activity in cell-free assays,[13] indicating that its mechanism of action is independent of direct radical scavenging. In summary, both N5NM15 and PAA show promising potential as novel multi-target agents for mitigating OS and inflammation related to NDs. These findings highlight their role in neuroprotective strategies and require further investigation into their mechanisms of action and potential clinical applications which may discover novel therapeutic targets and pathways.

3.5 Cholinesterase inhibitory activity in SH-SY5Y cells

The cholinesterase inhibitory activity of the compounds on AChE and BuChE enzymes was studied in undifferentiated SH-SY5Y cells using Ellman's assay. While none of the compounds showed significant inhibition of AChE activity (Fig. 12(A)), both the N5 conjugate ($p \leq 0.05$) and the N5NM15 nano-polyplex ($p \leq 0.01$) demonstrated significant inhibition of BuChE activity in these cells (Fig. 12(B)).

The reduced inhibitory activity could be due to the lower expression levels of AChE and BuChE in undifferentiated SH-SY5Y cells.[50,51] Differentiated SH-SY5Y cells, exhibiting mature neuron-like features and cholinergic neuronal phenotype, express higher levels of cholinesterase, potentially providing a more accurate model for assessing cholinesterase inhibitory activity.[52] Given the increasing role of BuChE in the later stages of AD, selective inhibition by N5NM15 highlights its potential in developing neuroprotective treatments for AD and other NDs. However, further studies using differentiated SH-SY5Y cells are necessary for understanding the inhibitory mechanism of N5NM15 nano-polyplex and to explore its therapeutic potential in targeting AChE and BuChE in NDs.

3.6. Inhibition of Aβ aggregation

In AD, the aggregation of toxic proteins, such as Aβ, is one of the hallmarks contributing to disease progression.[3,10] The inhibitory activity of N5NM15 and PAA against Aβ aggregation was demonstrated using the ThT assay (Fig. 13(A) and (B)). ThT binds to protein fibrils, emitting fluorescence, which is reduced when inhibitors prevent aggregation.[21]

The results showed that N5NM15 and PAA significantly reduced Aβ aggregation, by 10% and 20%, respectively ($p \leq 0.001$) (Fig. 13(A)). This reduction in aggregation was further confirmed using TEM (Fig. 13(B)). TEM images revealed dense fibrillar aggregates of Aβ in the control sample. When treated with N5NM15, PAA, and NAC, fewer Aβ fibrils were detected compared to Aβ alone.

Interestingly, the behaviour of PAA in this study contrasts with previous findings,[53] where a lower molecular weight (Mwt) PAA (14 000 Da) did not significantly affect Aβ aggregation. The use of a higher Mwt PAA (25 000 Da) appears to be a crucial factor contributing to its enhanced inhibitory activity. The higher Mwt PAA may enhance its ability to modulate Aβ aggregation through steric hindrance by providing a physical barrier that prevents Aβ from aggregating into toxic oligomers and fibrils. This steric hindrance or increased polymer size might also lead to improved binding interactions with Aβ peptides.

Furthermore, both N5NM15 and PAA are negatively charged, as is Aβ at physiological pH.[53] This similarity in charge would typically result in electrostatic repulsion, suggesting that the mechanism behind the inhibition of aggregation is more complex than simple charge-based interactions. Zang *et al.*,[54] developed a ratiometric fluorescent probe, oligo(fluorene-*co*-phenylene) (OFP), which was modified with a 1,8-naphthalimide (NA) derivative called OFP-NA-NO_2. This probe selectively recognized Aβ and effectively inhibited its self-assembly into fibrils through hydrophobic interactions, which may be attributed to the naphthalimide moiety, along with potential covalent binding. The active ester group on

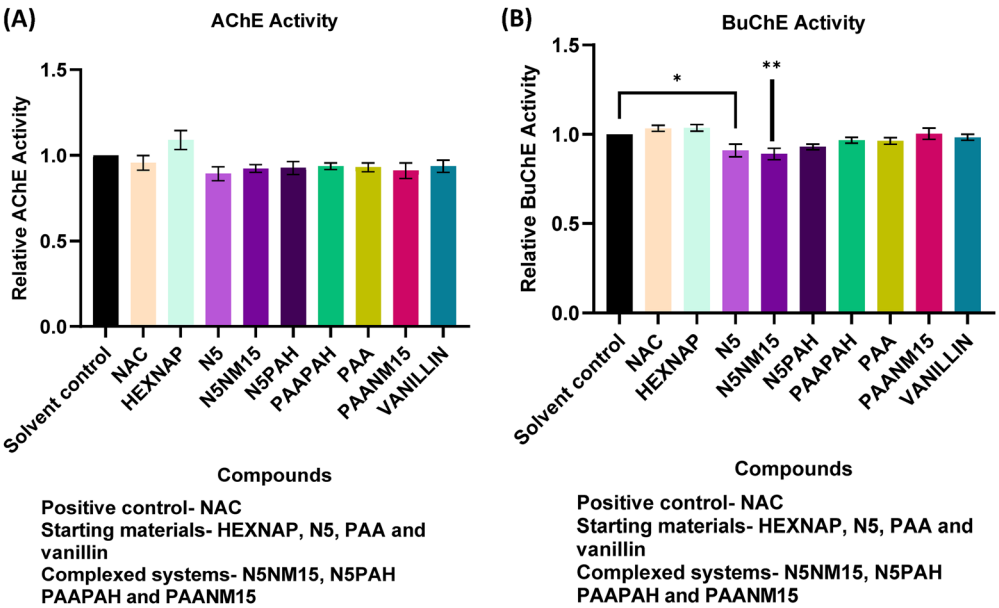

Fig. 12 Ellman's (A) AChE and (B) BuChE inhibitory activity of compounds in undifferentiated SH-SY5Y cells after 24 h of treatment. Data presented as mean ±SD (n = 3 independent experiments), significant difference *via* one-way ANOVA (***$p \leq 0.001$ for BuChE), and Dunnett's multiple comparisons tests. The final concentrations used were as follows: NAC and vanillin at 12.5 μg mL^{-1}; HEXNAP at 3 μg mL^{-1}; N5 and PAA at 44 μg mL^{-1}; PAANM15 at a ratio of 7.5 : 1 with a final concentration of 94 : 12.5 μg mL^{-1}; N5NM15, N5PAH, and PAAPAH at a ratio of 3.5 : 1 with a final concentration of 44 : 12.5 μg mL^{-1}.

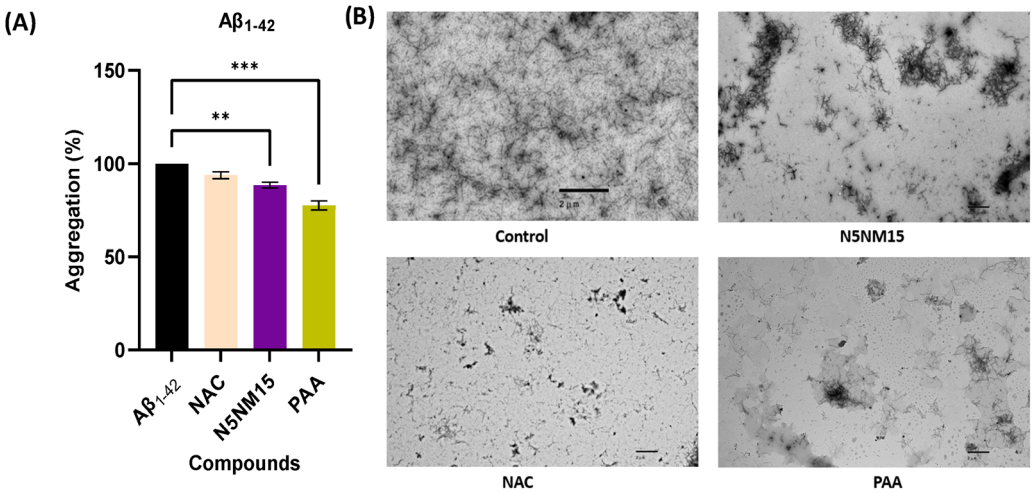

Fig. 13 (A) The inhibitory activity of N5NM15 and PAA against amyloid aggregation was measured by the ThT assay. Data presented as mean ± SEM (n = 3), significant difference *via* one-way ANOVA (***$p \leq 0.001$), and Dunnett's multiple comparisons tests. (B) TEM images showing the inhibition of $A\beta_{1-42}$ aggregation for representative compounds (scale bar = 2 μm). The final concentrations used were as follows: NAC at 12.5 μg mL^{-1}; PAA at 44 μg mL^{-1}; N5NM15 at a ratio of 3.5 : 1 with a final concentration of 44 : 12.5 μg mL^{-1}.

OFP-NA-NO_2 formed a covalent bond with the amino group on the lysine residue of Aβ, significantly disrupting the aggregation process and preventing the formation of Aβ fibrils. This finding suggests that targeting specific amino acid residues on Aβ can be an effective strategy to interfere with its aggregation.

However, under physiological aqueous conditions, the formation of covalent bonds between PAA and amino groups (*e.g.*, lysine residues of Aβ) is unlikely without the use of activating agents such as carbodiimides. Therefore, the inhibition of Aβ aggregation by N5NM15 is more plausibly attributed to non-covalent mechanisms. The presence of vanillin and HEXNAP in N5NM15 could contribute to its inhibitory effects by interacting with the hydrophobic regions of Aβ, preventing the aggregation of Aβ. Compounds with aromatic structures can disrupt π-stacking interactions between aromatic residues of the protein, further inhibiting Aβ aggregation.[21] Additionally, PAA could exert indirect effects by altering the microenvironment around Aβ, potentially affecting its aggregation pathway. Nonetheless, derivatisation of PAA with reactive esters, similar to the OFP-NA-NO_2 probe described by Zang *et al.*,[54] could be explored in future work as a strategy for enhancing covalent interaction with Aβ aggregation. Additionally, future studies could employ circular dichroism spectroscopy to confirm and characterise any structural changes in the Aβ.

These findings have significant implications for developing polymer-based therapeutics in treating AD and other NDs. By significantly inhibiting Aβ aggregation, N5NM15 and PAA show potential as therapeutic agents capable of mitigating amyloid pathology in the brain. However, further cell-based and *in vivo* studies and a deeper understanding of the underlying molecular mechanisms are crucial for advancing these findings toward clinical applications. These insights could pave the way for developing novel multi-target approaches for AD and other ND treatments.

4. Conclusion

This study highlights the therapeutic potential of a novel nano-polyplex, N5NM15, formulated by combining PAH–vanillin and PAA–HEXNAP conjugates, to target multiple pathological aspects of NDs. Both the N5NM15 nano-polyplex and PAA exhibited significant antioxidant activity, cholinesterase inhibition, and protective effects against hydrogen peroxide-induced OS in SH-SY5Y cells. Additionally, N5NM15 and PAA showed significant anti-inflammatory properties against LPS-induced inflammation and provided substantial protection against hydrogen peroxide-induced damage in BV-2 cells. Furthermore, their significant inhibition of Aβ aggregation, a key pathological hallmark of AD, suggests their potential to modulate key disease pathways. Overall, these results suggest that N5NM15 nano-polyplex and PAA have the potential to address multiple aspects of NDs, making them promising multi-target candidates for further investigation.

Author contributions

Nuruddin Mahadik: writing – original draft, visualization, methodology, investigation, formal analysis, data curation. Gemma A. Barron: supervision, writing – review & editing. Paul Kong Thoo Lin: supervision, writing – review & editing. Colin J. Thompson: conceptualization, supervision, funding acquisition, writing – review & editing.

Data availability

All data supporting the findings of this study are provided within the manuscript and its ESI.† No additional datasets were generated or analysed beyond those presented.

Conflicts of interest

There are no conflicts of interest disclosed by the authors. The author is solely accountable for the article's content and writing.

Acknowledgements

The authors would like to acknowledge the School of Pharmacy, Applied Sciences and Public Health at Robert Gordon University for providing their support for the completion of this work and Tenovus Scotland (G22.06 BG) for funding this work. The authors would like to further acknowledge Gillian Milne (University of Aberdeen) for TEM analysis. Cryo EM was performed by Dr Saskia Bakker at the Advanced Biomedical Imaging Facility (Warwick University). Imaging was funded by the Engineering and Physical Sciences Research Council (EPSRC) grant EP/V007688/1. We acknowledge the Midlands Regional Cryo-EM Facility, supported by MRC award reference MC_PC_17136.

References

1 A. Adamu, S. Li, F. Gao and G. Xue, *Front. Aging Neurosci.*, 2024, **16**, 1347987.
2 A. D. Gitler, P. Dhillon and J. Shorter, *Dis. Models Mech.*, 2017, **10**, 499–502.
3 N. Mahadik, G. A. Barron, P. Kong Thoo Lin and C. J. Thompson, *RSC Pharm.*, 2024, **1**, 161–181.
4 S. Negi, N. Khurana and N. Duggal, *Neurochem. Int.*, 2024, **177**, 105760.
5 S. Sveinbjornsdottir, *J. Neurochem.*, 2016, **139**, 318–324.
6 S. M. Hoy, *Drugs*, 2023, **83**, 359–365.
7 M. H. Ebell, H. C. Barry, K. Baduni and G. Grasso, *Ann. Fam. Med.*, 2024, **22**, 50–62.
8 D. Knez, N. Coquelle, A. Pišlar, S. Žakelj, M. Jukič, M. Sova, J. Mravljak, F. Nachon, X. Brazzolotto, J. Kos, J.-P. Colletier and S. Gobec, *Eur. J. Med. Chem.*, 2018, **156**, 598–617.
9 L. Blaikie, G. Kay and P. Kong Thoo Lin, *Bioorg. Med. Chem. Lett.*, 2020, **30**, 127505.
10 L. Blaikie, G. Kay and P. Kong Thoo Lin, *MedChemComm*, 2019, **10**, 2052–2072.
11 V. Nozal, P. Fernández-Gómez, A. García-Rubia, L. Martínez-González, E. P. Cuevas, E. Carro, V. Palomo and A. Martínez, *Biomed. Pharmacother.*, 2024, **175**, 116626.
12 C. Zhu, Y. Yang, X. Li, X. Chen, X. Lin and X. Wu, *Nano Res.*, 2022, **15**, 5173–5182.
13 N. Mahadik, G. A. Barron, P. K. Thoo Lin and C. J. Thompson, *Chem. Mater.*, 2024, **36**, 10514–10527.
14 A. D. Kulkarni, Y. H. Vanjari, K. H. Sancheti, H. M. Patel, V. S. Belgamwar, S. J. Surana and C. V. Pardeshi, *Artif. Cells, Nanomed., Biotechnol.*, 2016, **44**, 1615–1625.
15 W. W. Smith, *J. Neurosci.*, 2005, **25**, 5544–5552.
16 X. Tao, N. Li, F. Liu, Y. Hu, J. Liu and Y.-M. Zhang, *Heliyon*, 2018, **4**, e00730.
17 G. A. Barron, G. Bermano, A. Gordon and P. Kong Thoo Lin, *Eur. J. Med. Chem.*, 2010, **45**, 1430–1437.
18 D. Huang, B. Ou, M. Hampsch-Woodill, J. A. Flanagan and R. L. Prior, *J. Agric. Food Chem.*, 2002, **50**, 4437–4444.
19 M. Scipioni, G. Kay, I. Megson and P. Kong Thoo Lin, *Eur. J. Med. Chem.*, 2018, **143**, 745–754.
20 W. Sun, L. Chen, W. Zheng, X. Wei, W. Wu, E. G. Duysen and W. Jiang, *Toxicology*, 2017, **384**, 33–39.
21 D. D. Soto-Ortega, B. P. Murphy, F. J. Gonzalez-Velasquez, K. A. Wilson, F. Xie, Q. Wang and M. A. Moss, *Bioorg. Med. Chem.*, 2011, **19**, 2596–2602.
22 S. Kamiloglu, G. Sari, T. Ozdal and E. Capanoglu, *Food Front.*, 2020, **1**, 332–349.
23 L. Blaikie, G. Kay, P. Maciel and P. Kong Thoo Lin, *Eur. J. Med. Chem. Rep.*, 2022, **5**, 100044.
24 O. Boussif, T. Delair, C. Brua, L. Veron, A. Pavirani and H. V. J. Kolbe, *Bioconjugate Chem.*, 1999, **10**, 877–883.
25 R. K. Oskuee, E. Mohtashami, L. Golami and B. Malaekeh-Nikouei, *J. Exp. Nanosci.*, 2014, **9**, 1026–1034.
26 B. D. Monnery, M. Wright, R. Cavill, R. Hoogenboom, S. Shaunak, J. H. G. Steinke and M. Thanou, *Int. J. Pharm.*, 2017, **521**, 249–258.
27 S. K. Tripathi, Z. Ahmadi, K. C. Gupta and P. Kumar, *Colloids Surf., B*, 2016, **140**, 117–120.
28 F. Richter, K. Leer, L. Martin, P. Mapfumo, J. I. Solomun, M. T. Kuchenbrod, S. Hoeppener, J. C. Brendel and A. Traeger, *J. Nanobiotechnol.*, 2021, **19**, 292.
29 M. Danaei, M. Dehghankhold, S. Ataei, F. Hasanzadeh Davarani, R. Javanmard, A. Dokhani, S. Khorasani and M. R. Mozafari, *Pharmaceutics*, 2018, **10**, 57.
30 J. K. Bediako, E. S. M. Mouele, Y. El Ouardi and E. Repo, *Chem. Eng. J.*, 2023, **462**, 142322.
31 V. Bali, M. Ali and J. Ali, *Int. J. Pharm.*, 2011, **403**, 46–56.
32 V. Jolivel, S. Brun, F. Binamé, J. Benyounes, O. Taleb, D. Bagnard, J. De Sèze, C. Patte-Mensah and A.-G. Mensah-Nyagan, *Cells*, 2021, **10**, 698.
33 Z. Cockova, H. Ujcikova, P. Telensky and J. Novotny, *J. Biosci.*, 2019, **44**, 88.
34 C. Gollwitzer, D. Bartczak, H. Goenaga-Infante, V. Kestens, M. Krumrey, C. Minelli, M. Pálmai, Y. Ramaye, G. Roebben, A. Sikora and Z. Varga, *Anal. Methods*, 2016, **8**, 5272–5282.
35 M. Wagner, C. Pietsch, L. Tauhardt, A. Schallon and U. S. Schubert, *J. Chromatogr. A*, 2014, **1325**, 195–203.
36 F. Caputo, A. Arnould, M. Bacia, W. L. Ling, E. Rustique, I. Texier, A. P. Mello and A.-C. Couffin, *Mol. Pharmaceutics*, 2019, **16**, 756–767.
37 S. K. Filippov, R. Khusnutdinov, A. Murmiliuk, W. Inam, L. Y. Zakharova, H. Zhang and V. V. Khutoryanskiy, *Mater. Horiz.*, 2023, **10**, 5354–5370.
38 R. C. Murdock, L. Braydich-Stolle, A. M. Schrand, J. J. Schlager and S. M. Hussain, *Toxicol. Sci.*, 2008, **101**, 239–253.
39 M. Babič, D. Horák, P. Jendelová, K. Glogarová, V. Herynek, M. Trchová, K. Likavčanová, P. Lesný, E. Pollert, M. Hájek and E. Syková, *Bioconjugate Chem.*, 2009, **20**, 283–294.

40 S. Manju and K. Sreenivasan, *J. Colloid Interface Sci.*, 2012, **368**, 144–151.
41 I. G. Munteanu and C. Apetrei, *Int. J. Mol. Sci.*, 2021, **22**, 3380.
42 Z.-R. Chen, J.-B. Huang, S.-L. Yang and F.-F. Hong, *Molecules*, 2022, **27**, 1816.
43 J. Gao, N. Midde, J. Zhu, A. V. Terry, C. McInnes and J. M. Chapman, *Bioorg. Med. Chem. Lett.*, 2016, **26**, 5573–5579.
44 G. Mushtaq, N. Greig, J. Khan and M. Kamal, *CNS Neurol. Disord.:Drug Targets*, 2014, **13**, 1432–1439.
45 L. Zhong, J. Zhou, X. Chen, Y. Lou, D. Liu, X. Zou, B. Yang, Y. Yin and Y. Pan, *Sci. Rep.*, 2016, **6**, 22635.
46 A. F. Alkandari, S. Madhyastha and M. S. Rao, *Int. J. Mol. Sci.*, 2023, **24**, 12733.
47 M. Costa, J. Bernardi, T. Fiuza, L. Costa, R. Brandão and M. E. Pereira, *Chem. – Biol. Interact.*, 2016, **253**, 10–17.
48 C. R. A. Batista, G. F. Gomes, E. Candelario-Jalil, B. L. Fiebich and A. C. P. de Oliveira, *Int. J. Mol. Sci.*, 2019, **20**, 2293.
49 X. Chen, X. Zhou, X. Cheng, L. Lin, Q. Wang, R. Zhan, Q. Wu and S. Liu, *Molecules*, 2023, **28**, 3482.
50 L. Pulkrabkova, L. Muckova, M. Hrabinova, A. Sorf, T. Kobrlova, P. Jost, D. Bezdekova, J. Korabecny, D. Jun and O. Soukup, *Arch. Toxicol.*, 2023, **97**, 2209–2217.
51 S. Onder, L. M. Schopfer, W. Jiang, O. Tacal and O. Lockridge, *Neurotoxicology*, 2022, **90**, 1–9.
52 L. M. de Medeiros, M. A. De Bastiani, E. P. Rico, P. Schonhofen, B. Pfaffenseller, B. Wollenhaupt-Aguiar, L. Grun, F. Barbé-Tuana, E. R. Zimmer, M. A. A. Castro, R. B. Parsons and F. Klamt, *Mol. Neurobiol.*, 2019, **56**, 7355–7367.
53 A. Assarsson, S. Linse and C. Cabaleiro-Lago, *Langmuir*, 2014, **30**, 8812–8818.
54 Z. Zhang, Q. Yuan, M. Li, B. Bao and Y. Tang, *Small*, 2021, **17**, 2104581.